

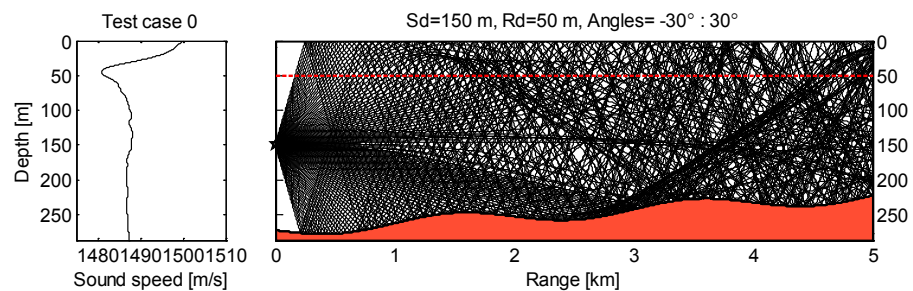
Report

Ray trace modeling of underwater sound propagation

Documentation and use of the PlaneRay model

Author

Jens Martin Hovem



SINTEF IKT
SINTEF ICTAddress:
Postboks 4760 Sluppen
NO-7465 Trondheim
NORWAYTelephone:+47 73593000
Telefax:+47 73592730postmottak.ikt@sintef.no
www.sintef.no
Enterprise /VAT No:
NO 948 007 029 MVA

Report

Ray trace modeling of underwater sound propagation

Documentation and use of the PlaneRay model

KEYWORDS:Acoustics
Underwater sound
propagation
Ray tracingVERSION
1.0DATE
2011-11-23AUTHOR
Jens Martin HovemCLIENT(S)
SINTEF ICTCLIENT'S REF.
Odd Kr. Ø. PettersenPROJECT NO.
90521023NUMBER OF PAGES/APPENDICES:
49**ABSTRACT**

PlaneRay is a ray tracing program for modeling of underwater acoustic propagation with moderately range-varying bathymetry and bottom parameters. The sound speed of the water may vary with depth, but not with range. The bottom can be a fluid sedimentary layer over an elastic half space with geo-acoustic properties that may vary with range. No rays are traced into the bottom, but the bottom interaction is modeled by local plane wave reflection coefficients. The model uses a unique sorting and interpolation routine to determine all eigenrays connecting a source with a number of receivers positioned on a horizontal line. For each eigenray, the model calculates the trajectories, travel times and amplitudes and constructs the complete frequency domain transfer function by coherent addition of all contributions of the multiple arrivals. Multiplying with the spectrum of a source signal and Fourier transformation of the product yields the time responses of the received signals. A unique feature of the model is that the contribution of the various multipath arrivals are evaluated separately, thereby enabling the user to study the structure of the field in detail. This report gives a description of the model and presents a number of illustrative cases. The accuracy of the ray model and the use of the plane wave reflection coefficients to represent the effects of a layered bottom are discussed by comparing the time and frequency domains solution of the ray model with the results from other established propagation models.

PREPARED BY
Jens M. Hovem

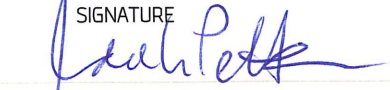
SIGNATURE

CHECKED BY
Idar L. N. Granøien

SIGNATURE

APPROVED BY
Odd Kr. Ø. Pettersen

SIGNATURE

REPORT NO.
A21539ISBN
978-82-14-04997-8CLASSIFICATION
UnrestrictedCLASSIFICATION THIS PAGE
Unrestricted

Document history

VERSION	DATE	VERSION DESCRIPTION
1.0	2011-11-23	Final

Table of contents

1	Introduction	4
1.1	A short history of the PlaneRay	5
2	Model description.....	5
2.1	Initial ray tracing and generation of ray history records	7
2.2	Eigenray determinations.....	8
2.3	Acoustic absorption in sea water.....	12
2.4	Boundary conditions at the surface and bottom interfaces.....	12
2.5	Source signature and directivity	14
3	Frequency domain transfer function and transmission loss	17
4	Time domain solutions.....	19
5	Some special considerations	21
5.1	The use of plane wave reflection coefficients	21
5.2	Caustics and turning points	23
5.3	The principle of reciprocity and its validity in ray modeling.....	24
6	High frequency applications	27
7	Accuracy considerations.....	27
7.1	Pekeris' waveguide	27
7.2	Elastic homogenous bottom.....	30
7.3	Distance from borders	32
7.4	Layered bottom	33
8	Producing results as function of depth.....	37
9	Conclusions	39
	References	40
A.1	Short users guide to PlaneRay	42
A.1.1	General	42
A.1.2	How to run the program.....	43
A.1.3	The input file.....	46

1 Introduction

Modeling of propagation conditions has always been an important issue in underwater acoustics and there exists a wide variety of mathematical/numerical models based on different approaches. The most common models are based on expansion in normal modes, models based on wave number integration technique or models based on the solution of the parabolic equation. For an overview of these models and for further references, see Jensen et al. (1993).

Ray tracing and ray theory derives from a high-frequency approximation of the wave equation and are conventionally considered appropriate only for active sonar frequencies. However, ray trace models may be more accurate than commonly believed, also for low frequency applications. Ray tracing models are also computationally efficient since the main calculation of ray trajectories is independent of frequency; the frequency enters only through the interaction with the boundaries, sea surface and sea floor, and can be introduced separately.

Ray theory and ray representation of the sound field gives a very physical description of the wave field that is easier to understand and interpret than other types of field descriptions. Because of this feature is often useful to use a ray model, in addition to other models, to obtain an understanding of the structure of the wave field and thereby giving guidelines for selecting the parameters of the other codes.

The use of ray tracing for propagation modeling is not new or original and many such models have been developed and presented in the literature earlier. For application in underwater relevant for the development of the PlaneRay model reference is made to the book by Officer and the articles of Westwood and Vidmar (1987) and Westwood and Tindle (1987) where ray tracing is applied for time-series simulation of shallow water propagation with a homogeneous fluid bottom. Stotts et al. (2004) also have reported modeling of transmission loss in range dependent environments using ray tracing. Other models that are frequently used and referred to are the Bellhop model [Porter (1991)] and the models of Abrahamson (2003) and Ivansson (2006).

An unique advantage with the PlaneRay model is that the contribution of the various multipath arrivals are evaluated separately, thereby enabling the user to study the field structure in detail. The method of sorting and classifications of rays have an additional advantage that it gives useful insight and understanding on how the sound field is composed and detailed information about the multipath structure. For instance, to know which part of the sound field has been reflected from the sea surface and which part has transmitted directly. These are all important features that enable the modeler to evaluate the reliability of the different propagation contributions. Thus the most valuable feature of the model may be the educational aspect and its usefulness in understanding the composition of an underwater wave field.

The intended application for the model was originally for passive sonar and in connection with geophysical research to gather seismo-acoustic properties of the sea bed. The model is currently used to model the propagation of airgun signal and seismic signal propagation in the water column in connections with studies how seismic surveys may impact marine life. The applications mentioned above requires modeling of low frequency signal, i.e. less than 1 kHz. More recently the applications have been extended toward higher frequencies in connection with studies of underwater acoustic communication. This application seems to fit the capability of the PlaneRay model since this model

resolves the multipath structure and distinguish between useful information carrying paths and paths the represents interference.

This report describes the PlaneRay model and presents typical examples of applications with for both range independent and range dependent scenarios. Results from testing and comparison with other propagation models are included. The discussions aim at illustrating the capability and limitations of the ray theory, and are partly of tutorial nature.

1.1 A short history of the PlaneRay model

The work with PlaneRay started in 2002 when the author was on sabbatical at Applied Research Laboratories (ARL) at Austin, Texas. The first reference to this work dates back to the ASA meeting in November 2002 [Hovem and Knobles (2002)] and to a paper presented at International Congress of Sound and Vibration (ICSV-2003) in Stockholm [Hovem and Knobles (2003)]. Later the work with the model was continued at the Norwegian Defence Research Establishment (NDRE). The objective was to develop a simple and relatively fast model to be used as the forward model in inversion schemes for determining sea bottom geoacoustic parameters from recorded acoustic transmission data. With colleagues from NDRE the model has been presented at several of conferences and in reports, by Smedsrud and Tollefsen (2007) and by Hovem (2007 and 2008). After leaving NDRE in July 2007 the work continued with correcting errors and several new products were developed to illustrate various aspect of wave propagation. PlaneRay model most valuable features may actually be the educational aspect and it usefulness in providing insights and understanding of the complexities of underwater acoustic wave fields. This report has been prepared as a part of the Underwater Acoustic Network (UAN) project in the 7th Framework Programme. ICT-Security joint call 2008-2011.

2 Model description

The algorithm can be considered as having three stages:

- (1) The initial ray tracing using a large number of rays to map out the entire sound field and record the ray history.
- (2) Sorting and interpolation to determine the ray parameters for the eigenrays connecting the source to the receivers. The ray parameters give the trajectories, travel times, and coordinates for surface and bottom interactions.
- (3) Synthesis of the acoustic field in time and frequency domains by coherent addition of the contributions of the eigenrays followed by Fourier transformation

The input information to the Plane Ray model is a sound speed profile (SSP), the range-dependent bathymetry with a description of the geoacoustic structure of the bottom, and the depths of the source and receivers. The receivers are assumed to be located on a horizontal line in the water. The sound speed profile in the water is limited to be a function of depth only, and is not allowed to vary in the horizontal direction. Rays are only traced to the water-sediment interface and not into the bottom; the acoustic effects of the bottom are represented by plane ray reflections coefficients. The bottom may be layered and in principle any number of fluid and elastic layers is allowed, but in the current version of the model only a fluid sedimentary layer over elastic half space is implemented. The thickness of the sediment layer and the geoacoustic properties of the bottom may vary with range.

The initial ray tracing is done by launching a relative large number of rays (typically 100 rays), with angles selected to cover the entire space between the source location and to the receivers on a horizontal line at the specified depth. The program determines the trajectories, travel times and amplitudes of all eigenrays connecting the source position to the receiver positions. The respective contributions of the eigenrays are thereafter coherently summed to produce the frequency-domain transfer function, followed by a Fourier transformation to obtain the time responses of the received signals.

The implementation used in the PlaneRay model is to divide the water column into a large number of layers with the same thickness Δz . This layer thickness is also used as the depth increment in the calculations. Generally, the accuracy of the modeling improves with a finer depth increment. Typically the layer thickness is chosen to be about 1%, or less, of the water depth. Within each layer, the sound speed is approximated with a straight line. In the layer $z_i < z < z_{i+1}$, the sound speed is thereby approximated to

$$c(z) = c_i + (z - z_i) g_i \quad (1)$$

where c_i is the sound speed at depth z_i , and g_i is the sound speed gradient in the layer,

$$g_i = \frac{c(z_{i+1}) - c(z_i)}{(z_{i+1} - z_i)}. \quad (2)$$

With constant sound speed gradient the rays in each layer follow circular arcs with a radius $P_i(z)$ given by the local sound speed gradient $g_i(z)$ and the ray parameter ξ ,

$$P_i(z) = -\frac{1}{\xi g_i(z)}. \quad (3)$$

The ray parameter is defined as:

$$\xi = \frac{\cos(\theta_s)}{c(z_s)} \quad (4)$$

where θ_s is the initial angle of the ray's trajectory at the source depth z_s where the sound speed is $c(z_s)$. After travelling through the layer from z_i to z_{i+1} the range increment is

$$r_{i+1} - r_i = -P_i(\sin \theta_{i+1} - \sin \theta_i) \quad (5)$$

which also can be written in the form

$$r_{i+1} - r_i = \frac{1}{\xi g_i} \left[\sqrt{1 - \xi^2 c^2(z_{i+1})} - \sqrt{1 - \xi^2 c^2(z_i)} \right] \quad (6)$$

and the travel time increment is

$$\tau_{i+1} - \tau_i = \frac{1}{|g_i|} \ln \left(\frac{c(z_{i+1})}{c(z_i)} \frac{1 + \sqrt{1 - \xi^2 c^2(z_i)}}{1 + \sqrt{1 - \xi^2 c^2(z_{i+1})}} \right). \quad (7)$$

The calculation of the trajectories and travel times using Equations (6) and (7) assumes that the curvature of a ray is finite, i.e. that the sound speed gradient is non-zero. In real life this will always be the case. However, for testing and in some other studies, it is useful to have the possibility of using a constant sound speed. In such cases Equation (6) and Equation (7) are replaced with

$$r_{i+1} - r_i = \frac{|z_{i+1} - z_i|}{\tan \theta_{i+1}}. \quad (8)$$

$$\tau_{i+1} - \tau_i = \frac{|z_{i+1} - z_i|}{c_{i+1} \sin \theta_{i+1}}. \quad (9)$$

When the water depth varies with range, the ray parameter is no longer constant, but changes with the bottom inclination angle from θ_{in} to θ_{out} , and depending on the sign of the ray angle and the angle of bottom slope α according to

$$\xi_{out} = \frac{\cos(\theta_{out})}{c} = \frac{\cos(\theta_{in} \pm 2\alpha)}{c}. \quad (10)$$

The acoustic intensity is calculated using the principle that the power within a space limited by a pair of rays with initial angular separation of $d\theta_0$ and centered on the initial angle θ_0 , will remain between the two rays regardless of the rays' paths. The acoustic intensity as function of horizontal range $I(r)$ is, according to this principle, given by

$$I(r) = I_0 \frac{r_0^2 \cos \theta_0}{r \sin \theta} \left| \frac{d\theta_0}{dr} \right|. \quad (11)$$

In Equation (11), the initial angle at the source is denoted θ_0 and θ is the ray angle at the receiver position, which is at the horizontal range r from the source. The equation predicts infinite intensity under two conditions, when $\theta = 0$ and when $dr/d\theta_0 = 0$. The first condition signifies a turning point where the ray path becomes horizontal; the second condition occurs at points where an infinitesimal increase in the initial angle of the ray produces no change in the horizontal range traversed by the ray. The locations where $dr/d\theta_0 = 0$ are called caustics with infinite intensity as predicted by Equation (11). In reality there is focusing of energy to a very high level, but the actual level is not determined by classical ray theory. The problem with calculation of the acoustic field at caustics and turning points represents a limitation of ray theory that will be presented later.

2.1 Initial ray tracing and generation of ray history records

The equations in the preceding section are applied to calculate the trajectories for a number of rays spanning the whole range of initial angles that are relevant for the actual studies. All receivers are assumed to be at the same depth. For each ray the ranges and the travel time to the intersections with the receiver depth are detected together with the angles and coordinates of where the rays have been reflected from the bottom and surface, and where the rays have gone through turning points. All this information, the ray history, is stored in the computer for later look up. Since the sound speed profile

and the bathymetry are supposed to be fixed the ray tracing calculation needs only to be done once for each scenario.

Figure 1 shows a typical example with an undulating sloping bottom with a sediment layer of 10 meter over hard bedrock. The sound speed profile is a typical summer for northern waters. Figure 1 show 120 ray trajectories from a source at 150 m depth with initial angles in the range from -30° to $+30^\circ$.

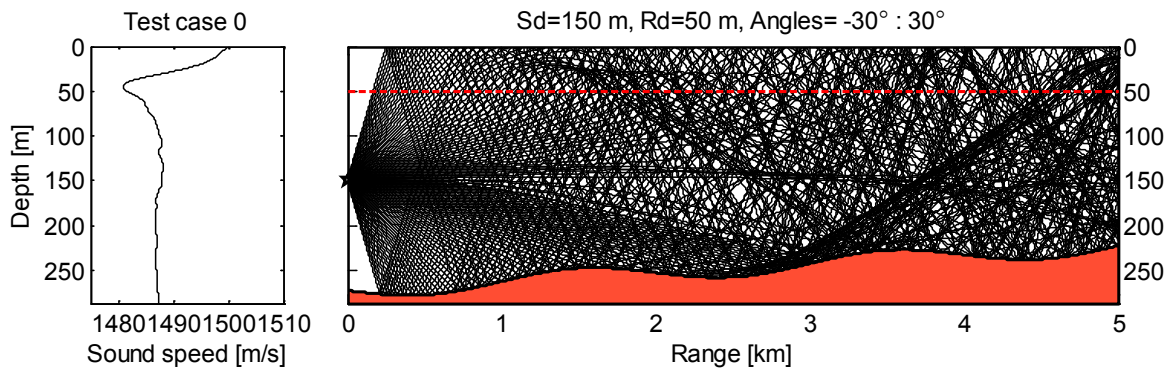


Figure 1 Sound speed profile and ray traces for a typical case. The source depth is 150m and the red dotted line indicates the receiver line at a depth of 50 m. The initial angles of the rays at the source are from -30° to 30° .

2.2 Eigenray determinations

Figure 2 displays parts of the ray history as function of initial angle at the source. The two plots show the ranges and travel times to where the rays cross the receiver depth line. A particular ray may intersect the receiver depth line, (marked by the red dashed line in Figure 1) at several ranges. For instance the plots in Figure 2 show that at the range of 2 km there are 11 eigenrays. By reading the range-angle plot in 0 the initial angles of these rays are approximately found to be 5.9° , 9.6° , 22° , 24° for the positive (down going) rays and -2.0° , -3.6° , -7.4° , -15.0° , -17.0° , -25.0° , -27.0° , for the negative (up-going waves). However, the values found in this way are often not sufficiently accurate for the determination of the sound field, and Equation (11) in particular. Further processing is therefore needed to obtain more accurate results. The approach of achieving higher accuracy is based on sorting the different rays into groups or classes followed by interpolation.

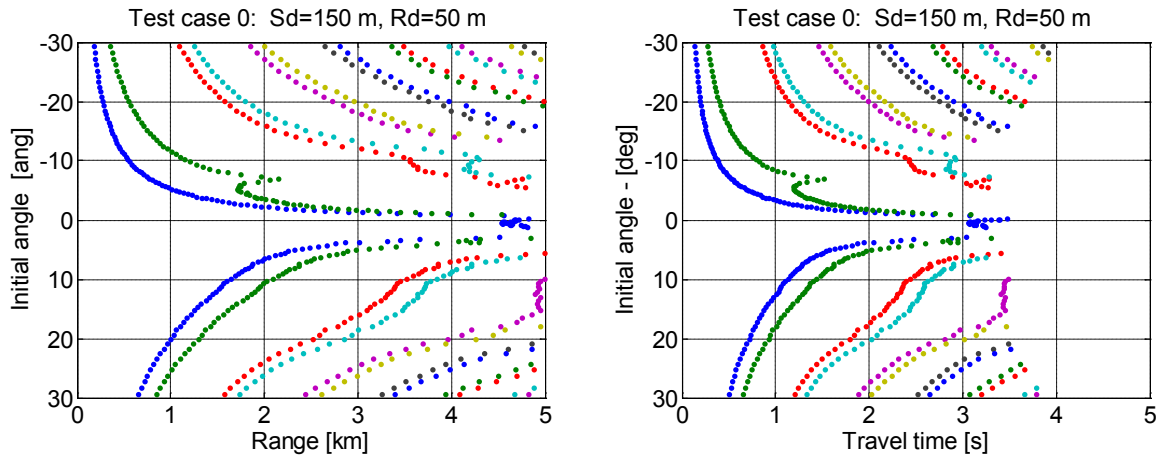


Figure 2 Ray history of the initial ray tracing in Figure 1 showing range (left) and travel time (right) to the receiver depth as function of initial angle at the source.

Using the recorded ray history, the rays are sorted into classes with similar path characteristics and ray history. The classification is by the sign of the initial angle of ray, by the numbers of reflections at the bottom and sea surface and by the number of upper and lower turning points the ray has experienced. As a ray propagates from the source position it builds a six- element vector of the form:

[Initial-angle Target-count Bottom-count Surface-count, Upper-turning-count, Lower-turning-count].

Each time the ray strikes the bottom or, the sea surface, or goes through a turning point, the relevant counter is increased with one and when the ray intersects the receiver depth line the target counter is updated. The different classes of rays and ray history are defined in Table 1. In the special case of a constant sound speed there will be five classes and these are the classes 1, 2, 3, 4 and 5. For an arbitrary sound speed there may be upper- and lower turning points, which in combination with bottom and surface reflections define the other classes. With constant water depth the number of possible combinations or classes is limited to the seven classes defined in Table 1. With range dependent bathymetry there may be additional classes with both turning points and bottom/surface reflections. The model will search for these classes separately for situation where no coincidence with the classes of Table 1 is found.

When the rays and the ray history have been classified and sorted according to Table 1, the next step is to interpolate on each group of rays separately. Successful application of interpolation processing requires that the ranges to the receiver depth intersection increase or decrease monotonically with the increase in initial start angle so that range versus angle is single-valued function. If this is not the case, which will occur at the caustics (discussed later), the ranges as a function of start angle are divided into branches so that the each branch is a monotonic and single-valued function.

Table 1 Ray classification and history

Class	Bottom	Surface	
Class 1	0	0	Direct ray
Class 2	n-1	n	Negative start angle
Class 3	n	n	Negative start angle
Class 4	n	n	Positive start angle
Class 5	n	n-1	Positive start angle
Class	Bottom	Upper turning points	
Class 6	n	n+1	Negative start angle
Class 7	n	n	Negative start angle
Class 8	n	n	Positive start angle
Class 9	n+1	n	Positive start angle
Class	Surface	Lower turning points	
Class 10	n+1	n	Negative start angle
Class 11	n	n	Negative start angle
Class 12	n	n	Positive start angle
Class 13	n	n+1	Negative start angle
Class	Upper turning points	Lower turning points	
Class 14	n+1	n	Negative start angle
Class 15	n	n	Negative start angle
Class 16	n	n	Positive start angle
Class 17	n	n+1	Positive start angle

In most cases the eigenrays are determined by one simple interpolation yields values that are sufficiently accurate for most application, but, that depend on the complexity of the situation with respect to the bathymetry and the sound speed profile. Generally, the accuracy increases with increasing density of the initial angles at the cost of longer computation times. It is advisable to check the accuracy of the eigenray determination before proceeding with the acoustic field calculations. For more complicated situations the model also contains an advanced option to produce more accurate results for selected ranges where the initial eigenray results are deemed not having sufficient accuracy. After the first estimate of the eigenray is found, the trajectory of this ray is calculated and the difference between the actual range and the desired range to receiver depth intersection is determined and compared with a user specified threshold value. This process is repeated iteratively until an acceptable error limit is achieved, or until the specified number of iterations is reached. Figure 3 shows examples of eigenrays traces with rays to receivers located at 2.0 km and 4.0 km from the source for the scenario shown in Figure 1. To a receiver at 2.0 km there are a total of 11 eigenrays, spanning the range of initial angles from -29° to 25° , and to receiver at 4.0 km there are 21 eigenrays.

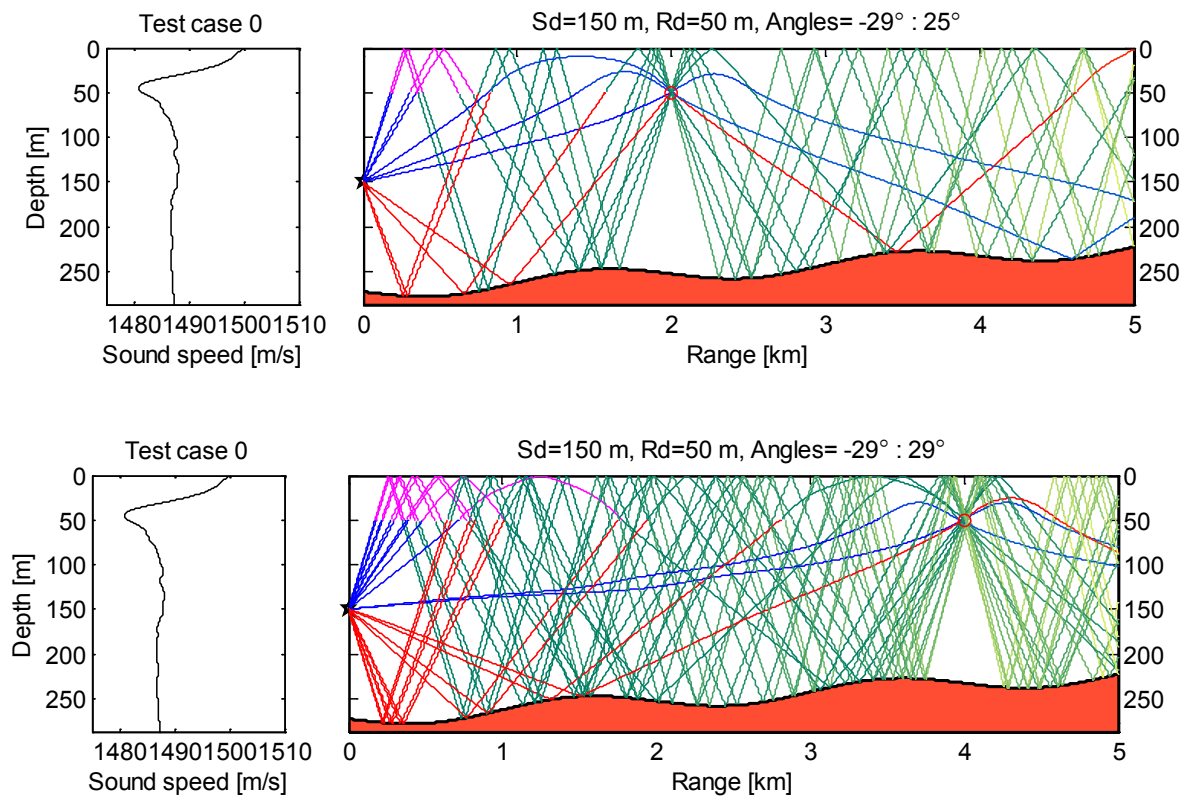


Figure 3 Eigenrays from a source at 150 m depth to a receiver at 50 m depth and distance of 2.0 km and 4.0 km distance from the source.

2.3 Acoustic absorption in sea water.

The model includes the standard acoustic absorption in sea water calculated by the semi-empirical formulae by Francoise and Garrison (1982). This equation gives sound absorption as function of frequency, temperature, salinity, depth, and pH value. Figure 4 shows the absorption calculated with the values for a water temperature of 10°C, atmospheric pressure of one atmosphere (surface), salinity of 35 pro mille, and *pH* value of 7.8. The figure shows the total absorption and the contributions of the various components causing acoustic absorption.

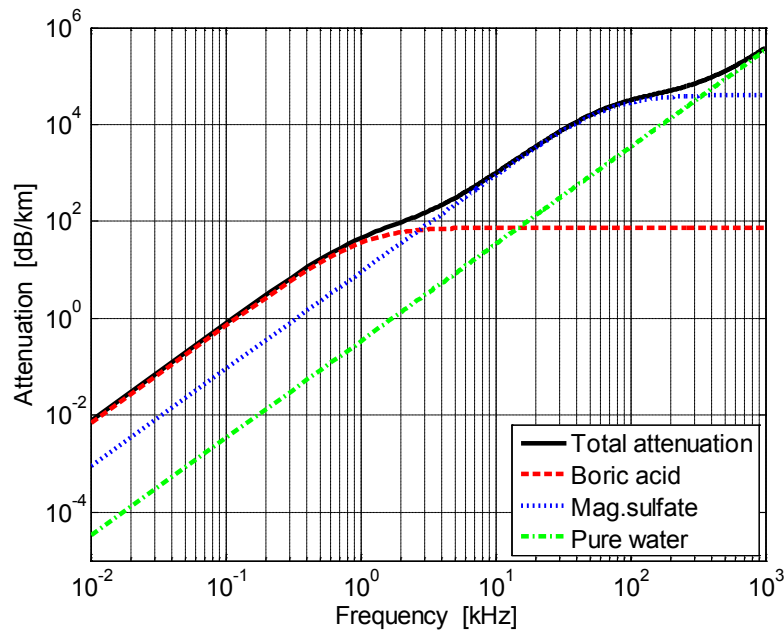


Figure 4 Acoustic attenuation (dB/km) for fresh and salt water, plotted as function of frequency (kHz) for water temperature of 8°C, atmospheric pressure of one atmosphere (surface), salinity of 35 pro mille, and *pH* value of 7.8. The legend indicates the various contributions to the attenuation.

2.4 Boundary conditions at the surface and bottom interfaces

Each ray separately has to satisfy the boundary conditions at the sea surface and the bottom. This is accomplished by the use of plane wave reflection coefficient.

The sea surface reflection coefficient is -1 for a flat even sea surface. For a sea surface with ocean waves, the rough surface the reflection coefficient is set to

$$R_{coh} = \exp \left[-2 \left(\frac{2\pi}{\lambda} \sigma_h \sin \theta \right)^2 \right]. \quad (12)$$

The rough surface reflection loss is defined as

$$R_{coh} = \exp \left[-2 \left(\frac{2\pi}{\lambda} \sigma_h \sin \theta \right)^2 \right]. \quad (13)$$

In this expression σ_h is the rms wave height in m, λ is the acoustic wavelength and θ is the grazing angle. Figure 5 shows the rough surface reflection loss as function of grazing angle, calculated for a wave height of 0.5 m and the frequencies of 50 Hz, 100 Hz, 200 Hz and 400 Hz.

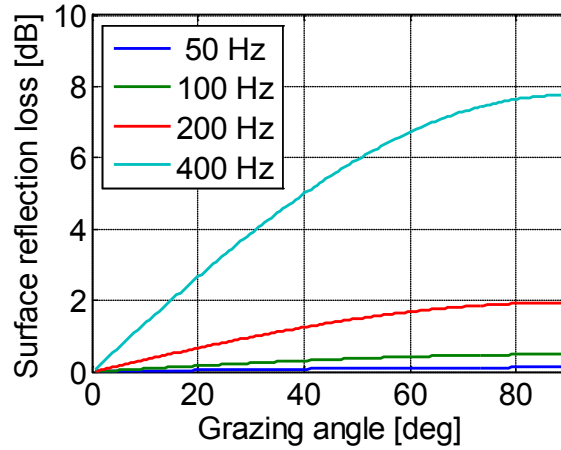


Figure 5 Reflection loss of rough sea surface with rms. wave height of 0.5 m as function of grazing angle, for the frequencies of 50 Hz, 100Hz, 200 Hz and 400 Hz.

As stated earlier no rays are traced into the bottom and the effects of a layered bottom are described entirely by plane wave ray reflection coefficients. In the current implementation the bottom is modeled with a fluid sedimentary layer over a homogeneous solid half space. The reflection coefficient of a bottom with this structure is

$$R_b = \frac{r_{01} + r_{12} \exp(-2i\gamma_{p1}D)}{1 + r_{01}r_{12} \exp(-2i\gamma_{p1}D)} \quad (14)$$

where γ_{p1} is the vertical wave number for sediment layer and D is the thickness of the sediment layer. The reflection coefficient between the water and the sediment layer, r_{01} , is given as

$$r_{01} = \frac{Z_{p1} - Z_{p0}}{Z_{p1} + Z_{p0}} \quad (15)$$

and r_{12} is the reflection coefficient between the sediment layer and the solid half space,

$$r_{12} = \frac{Z_{p2} \cos^2 2\theta_{s2} + Z_{s2} \sin^2 2\theta_{s2} - Z_{p1}}{Z_{p2} \cos^2 2\theta_{s2} + Z_{s2} \sin^2 2\theta_{s2} + Z_{p1}} \quad (16)$$

In Equations (15) and (16) Z_{ki} is the acoustic impedance for the compressional ($k=p$) and shear ($k=s$) waves in water column ($i=0$), sediment layer ($i=1$) and solid half-space ($i=2$), respectively. The grazing angle of the transmitted shear wave in the solid half-space is denoted θ_{s2} .

Figure 6 shows two examples of the bottom reflection loss as function of angle and frequency for a bottom with a sediment layer with the thickness $D = 5$ m, density 1500 kg/m^3 and sound speed 1700 m/s , over a homogeneous half space. In plot at the left side of Figure 6 the elastic half space has a sound speed of 3000 m/s , the shear speed is 500 m/s and the density is 2000 kg/m^3 . In the right-hand plot the same parameters are 4700 m/s , 2200 m/s and 2500 kg/m^3 .

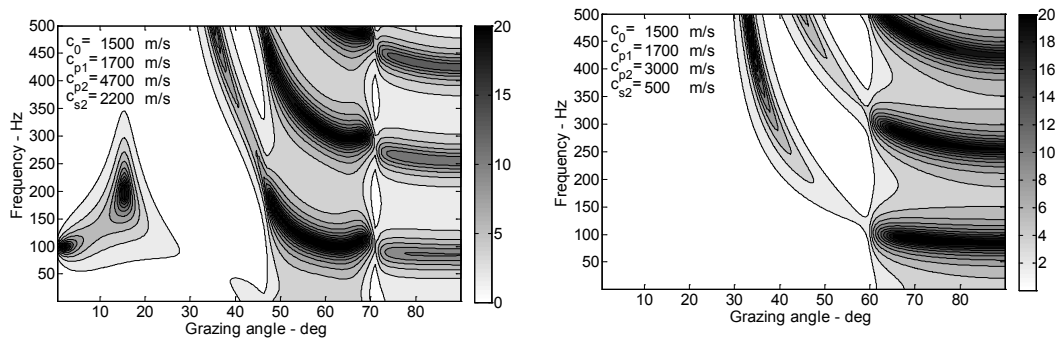


Figure 6 Bottom reflection loss (dB) as function of frequency and incident angle for: a 5 m sediment layer with sound speed of 1700 m/s and density 1800 kg/m^3 over a homogenous solid half space with: (Left) compressional speed 3000 m/s , shear speed 500 m/s and density 1800 kg/m^3 , (Right) compressional speed 4700 m/s , shear speed 2200 m/s and density 2500 kg/m^3 . All waves have the same attenuations of $0.5 \text{ dB/wavelength}$.

In the case of a low speed elastic half space (left-hand plot), the critical angle changes from 60° at very low frequencies to 28.1° at high frequencies, the two angles are given by the sound speed in the water and the two bottom sound speed of 3000 m/s and 1700 m/s . The small, but significant, reflection loss at lower angles is caused by shear wave conversion and bottom absorption. In the plot at the right side there are two compressional critical angles at 18.1° and 71.4° and one shear critical angle at 47.0° . In addition, there is a plateau of high reflection loss at low angles and frequencies with peaks at about 20° and 0° . These anomalous high values are caused by excitation of interface wave at the boundary between the sediment layer and the elastic half space. The reader may consult the works by Hovem and Kristensen (1992), Tollefsen (1998) and Ainslie (2003) for more information on this phenomenon.

2.5 Source signature and directivity

The specification of the source signal may be considered composed of two parts; (1) the modeling of a single source function, and (2) the directivity of acoustic transmitter. According to linear system theory, the complete source spectrum in frequency and directions is

$$H(\omega, \theta) = S(\omega) A(\omega, \theta). \quad (17)$$

$S(\omega)$ is the frequency function of the source and $A(\omega, \theta)$ is the directivity as function of frequency and the elevation angle. Note that the model is 2-dimensional (range and depth) and the azimuth angle is not included.

The user has to specify the source function either in time and frequency domain. This could be, for instance by loading a recorded signal, or by specifying the source signal by programming an expression. As a default, PlaneRay is equipped with a standard time function in the form of a Ricker pulse and the directivity of a linear horizontal array with N_e elements in regular spacing Δx of identical omni-directional sources.

The default choice of source signal is a Ricker pulse, an example is shown Figure 7 showing both the time signal and the frequency spectrum. In this case the peak of the main frequency spectrum is at 50 Hz, but the peak frequency can be changed, and other source function ,may be modelled by the user.

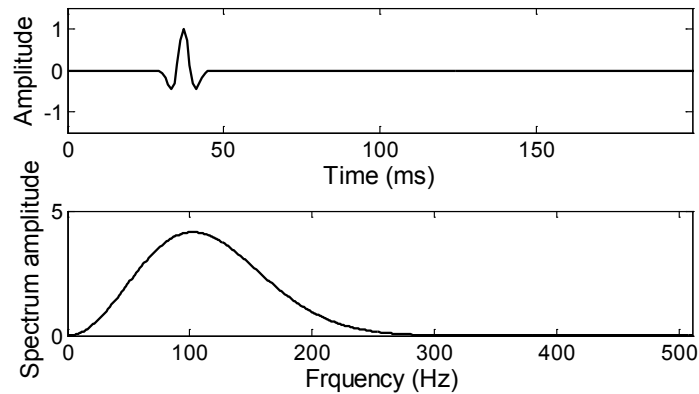


Figure 7 Ricker time pulse and frequency function

The simplest way to introduce a (vertical) directivity is simply to include only initial start angles within the beam width of the source. If this is not satisfactory the model is set up with a facility for user-specified directivity by modifying the relevant subroutine.

To illustrate this approach consider the modelling of a line array with N_e simple sources, regular spaced with distance Δx (in meters). With the acoustic frequency $\omega=2\pi f$ and wave length $\lambda=c/f$, the directivity in the farfield of a such horizontal array is

$$A(\omega, \theta) = N_e \left\{ \frac{\sin \left[\pi \frac{N_e \Delta x}{\lambda} \cos \theta \right]}{N_e \sin \left[\pi \frac{\Delta x}{\lambda} \cos \theta \right]} \right\}. \quad (18)$$

For a vertical array with the same specification the directivity pattern is rotated 90 degrees and can be expressed as

$$A(\omega, \theta) = N_e \left\{ \frac{\sin \left[\pi \frac{N_e \Delta x}{\lambda} \sin \theta \right]}{N_e \sin \left[\pi \frac{\Delta x}{\lambda} \sin \theta \right]} \right\}. \quad (19)$$

Figure 8 shows two examples of directivity diagrams, calculated by Equation (18) for $N_e=8$ elements spaced with $\Delta x = 10$ m and for the frequencies of 50 Hz and 150 Hz. Notice the repeated main lobe for 150 Hz, which occurs when the spatial sampling theorem is not satisfied, i.e. when $\Delta x > \lambda/2$.

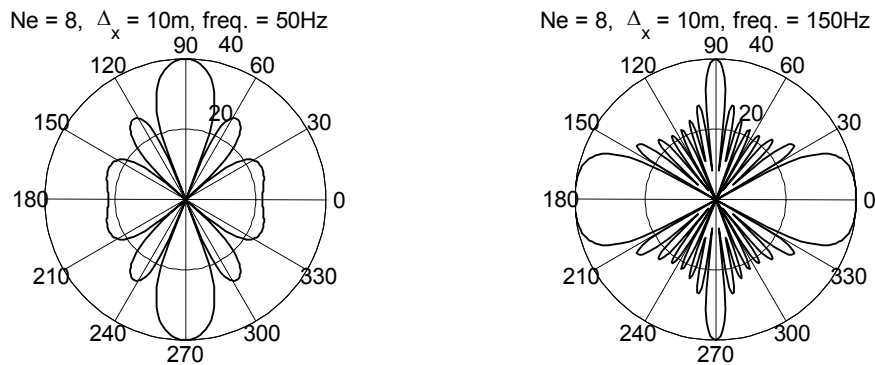


Figure 8 Directivity pattern as function of the elevation angle θ for a horizontal array with $N_e=8$ elements spaced at $\Delta x=10$ m for the frequencies of 50 Hz and 150 Hz.

These figures demonstrate that the directivity of an array is a complicated function of frequency. When we are dealing with transient and broad band frequency signal it is important to calculate the frequency-angle spectrum of Equation (17) for all frequencies of the source function if we want to calculate the time-domain response by Fourier transform of the frequency function.

Figure 9 provides an illustration of the time response of a horizontal array with $N_e=8$ elements with a constant spacing Δx of 15 m. The figure shows the direct signal to a number of receivers 100 m below the array and at horizontal distance from 10 m to 100 m. The transmitted signal is a Ricker pulse with max frequency 100 Hz. At the shortest distances, which is almost straight below the array the received signals are almost identical to the transmitted Ricker pulse, whereas the received signals at longer distances are spread out in time and consequently has considerable lower peak amplitude. This is in agreement with observations in Figure 8 since the receiver at 10 m correspond to an angle θ equal 86 ° and the receiver at 100 m is at an angle of 45°.

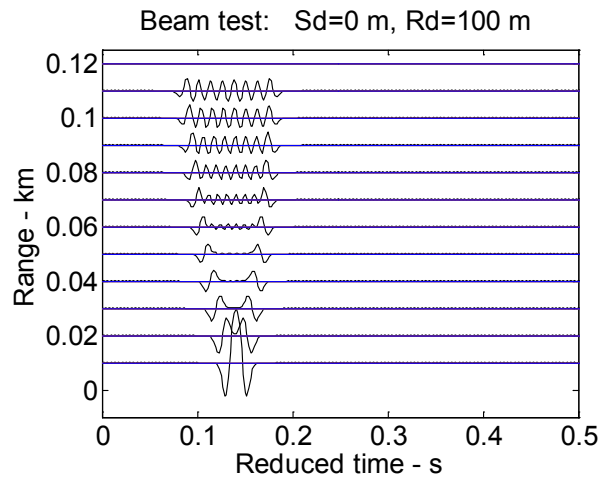


Figure 9 The direct signal from a transmitting array with 8 elements at 25 m spacing. The receivers are 100 m below the array at horizontal distance from 10 m to 100 m.

3 Frequency domain transfer function and transmission loss

The total wave field at any point along the receiver line is calculated in the frequency domain by coherent summation of all the eigenray contributions. The first step in the calculation of the frequency domain transfer function is to determine the geometrical transmission loss of each of the multipath contributions by applying Equation (11) to the sorted range-angle values. Figure 10 shows the geometrical transmission for the various multi paths for the example we are considering. Note the values at ranges of 1750 m, 3000 m and 4000 m, these minima in transmission loss represent the very high sound intensities at caustics and turning points to be discussed later.

The total transmission loss is obtained by adding the multipath contributions coherently in frequency domain taken into account the phase shifts associated the travel times from the interpolated history of the travel times. Also the acoustic absorption of sound in water is included at this point in the process and independent of each frequency component. Figure 11 shows an example where the transmission loss (in dB) as function of range has been calculated for the frequencies of 25 Hz, 50 Hz, 100 Hz and 200 Hz. The dashed black line indicates the geometrical spreading loss, which is added for comparison and given by,

$$TL_{geo} = 10 \log(r / r_0) + 20 \log(r). \quad (20)$$

In his case we have used r_0 =water depth at source location, which in this case is 200 m.

The synthesis of the received signals is performed in the frequency domain by multiplying the frequency spectrum of the source signal by the transfer function of each of the eigenrays and summing all the significant contributions.

Symbolically this operation can be expressed as

$$H(\omega, r) = \sum A_n B_n(\omega) S_n(\omega) T_n \exp(i\omega\tau_n). \quad (21)$$

Equation (21) expresses the transfer function $H(\omega, r)$ to a distance r from the source at the angular frequency ω as a sum over the N eigenrays that are included in the synthesis. A_n is the geometrical spreading, defined in Equation (11), B_n , and S_n , are the combined effects of all bottom reflections and surface reflections, respectively, T_n , is -90° phase shift associated with caustics and turning points, and τ_n is the travel time.

Figure 11 shows an example where the transmission loss (in dB) as function of range has been calculated for the frequencies of 25 Hz, 50 Hz, 100 Hz and 200 Hz. The dashed black line indicates the geometrical spreading loss, which is added for comparison and given by

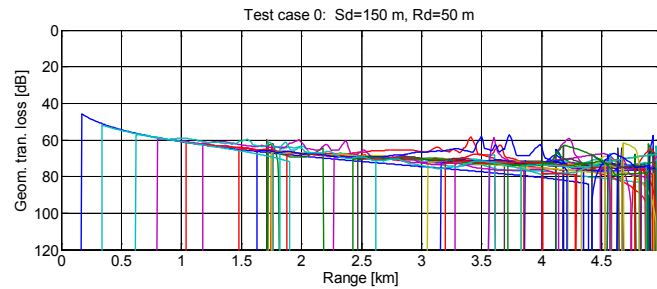


Figure 10 Geometrical transmission loss for the multipath contributions as function of range

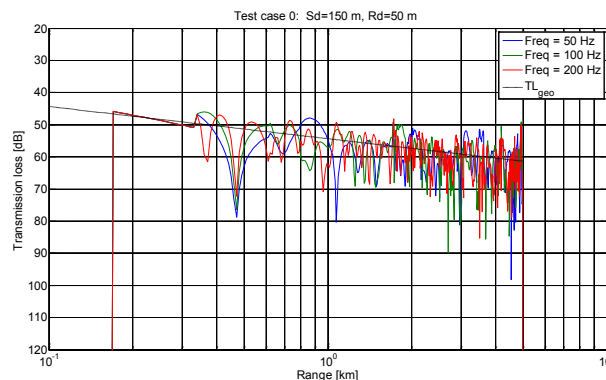


Figure 11 Transmission loss as function of range calculated for the frequencies of 50 Hz, 100 Hz, and 200 Hz. The dashed black line indicates the result of a simple formula for a geometrical spreading loss function of Equation (20).

4 Time domain solutions

The time domain solution is obtained after multiplication with the frequency function of a source signal and by an inverse Fourier transform of the product. This requires that the user defines a source signal, a sampling frequency (f_s) and a block length ($nfft$) of the Fourier transform. In the basic PlaneRay model only a simple Ricker pulse is implemented as a source pulse. (The user may easily add other source signals by modifying the relevant subroutine. Figure 7 shows a Ricker pulse and its frequency spectrum. In this case the centre frequency of the pulse is 100 Hz, but this parameter can be chosen by the user. The recommend minimum sampling frequency f_s of such a pulse is about 10 times the centre frequency. The total duration of the time window (T_{max}) after Fourier transform is

$$T_{max} = nfft / f_s . \quad (22)$$

It is very important that $nfft$ and f_s are selected so that Fourier time window, T_{max} , is larger than the actual length or duration of the signal. In reality the real time duration of the received signal is often not known in advanced and therefore the user may have to experiment with different values to find appropriate values for of $nfft$ and f_s . The program estimates the length of the impulse response and issues a warning when the received signal may be longer that the T_{max} of Equation (22).

Figure 12 shows a number of time responses as function of range and time. The time scale is in real time, i.e. the total time between emissions from the source to the pulse is at the receiver. A more convenient plot is shown in Figure 13 where the same time response are plotted as function of reduced time, defined as

$$t_{red} = t_{real} - \frac{r}{c_{red}} . \quad (23)$$

In Equation (23), t_{real} and t_{red} are the real and reduced times, respectively, r is range and c_{red} is the reduction speed. The actual value of c_{red} is not important as long as the chosen value results in a good display of the time responses.

Figure 12 also demonstrates the effect of the sorting approach of the PlaneRay model and that the various multipath arrivals are calculated separately and can be studied independently. In this case there are direct arrivals, followed by surface reflected and refracted arrivals at the turning points. The various multipath arrivals are color coded as indicated in the legend.

This is particularly useful when dealing with transient signal and broad band signal, especially when knowledge of the multipath structure is important. In many such situations the only the direct arrival or the refracted arrivals in the water column may carry the useful signals and all the other represents interference. Notice again the high sound pressure values caused by the caustics at 3 km, 6, km and 7 km., which are apparent in both plots. Caustics are treated more in detail in section 5.2.

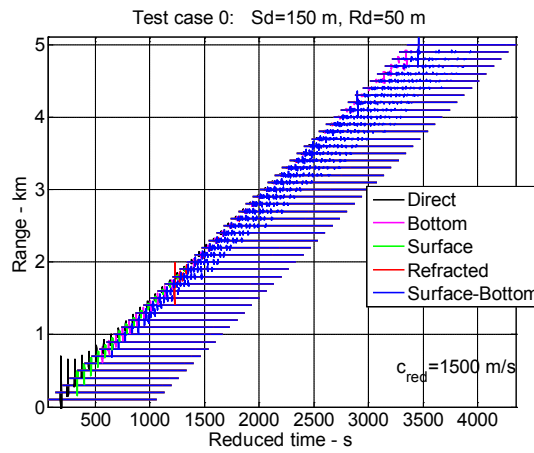


Figure 12 Received time responses as function of range and plotted as functions of real time.

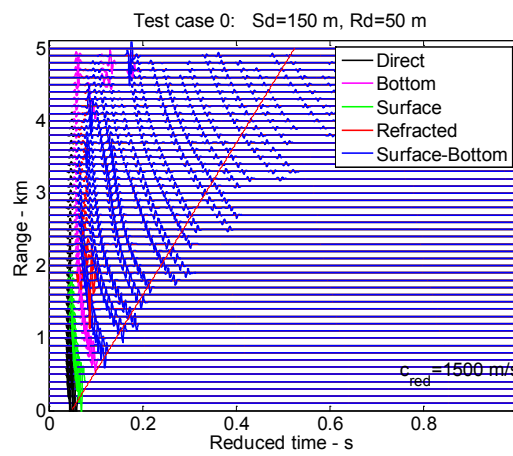


Figure 13 Received time responses as function of range and plotted as functions of reduced time.

5 Some special considerations

In this section we discuss some issues that are important for the application of ray theory to acoustic propagation modeling.

5.1 The use of plane wave reflection coefficients

A fundamental assumption of model is that the interactions with the boundaries are adequately described by plane wave reflection coefficient. In this section the validity of this assumption is investigated

Consider the situation depicted in Figure 14 where the source and the receiver are located at heights z_r and z_s above an interface between two media 1 and 2 with sound speeds c_1 and c_2 , and densities ρ_2 and ρ_1 , respectively.

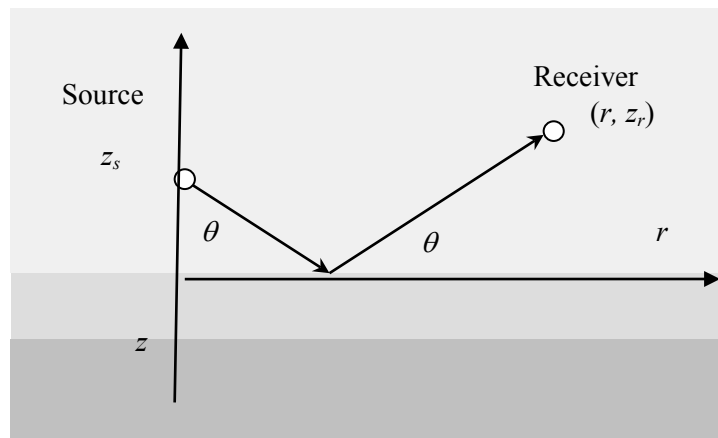


Figure 14 The point source is at height z_s and the receiver is at height z_r above the interface between two media. The horizontal distance between the source and receiver is r . The arrows indicate the ray paths in the specular direction.

The general expression for the reflected field is given in text books, as an integral for instance over horizontal wave numbers k , [Brekhovskikh, and Lysanov (2003)] as

$$\Phi_{ref}(r, z_r, \omega) = \frac{S(\omega)}{8\pi i} \int_0^{\infty} \Re(k) \frac{\exp(i\gamma_1 |z_r + z_s|)}{\gamma_1} k H_0^{(1)}(kr) dk. \quad (24)$$

$\Phi_{ref}(r, z_r, \omega)$ is the reflected field due to point source with frequency ω and source strength $S(\omega)$, $\Re(k)$ is the reflection coefficient. $H_0^{(1)}(kr)$ is the Hankel function of first kind, which represents a wave progressing in the positive r -direction. The horizontal wave number k is related to the grazing angle θ by

$$k = \frac{\omega}{c_1} \cos \theta. \quad (25)$$

Equation (24) states that the field is given as an integral over all horizontal wave numbers, or as consequence of Equation (25), an integration over all real and the imaginary angles.

Consider now the situation where $\Re(k) = \Re$ is constant and independent of k or the angle. The integral in Equation (24) then becomes a standard integral and the exact result can be expressed as

$$\Phi_{ref}(r, z_r, \omega) = \frac{S(\omega)}{4\pi R_1} \Re \exp(ikR_1) \quad (26)$$

where

$$R_1 = \left[r^2 + (z_s + z_r)^2 \right]^{\frac{1}{2}}. \quad (27)$$

According to Equations (26) and (27) the reflected wave is identical to an outgoing spherical wave from the image of the source in the mirror position of the real source and modified by the constant reflection coefficient \Re . The situation with a constant reflection coefficient is valid for perfectly flat sea surface where the reflection coefficient is equal to -1 for all angles of incidence. Thus the reflection from a smooth sea surface is accurately described by a plane wave reflection coefficient.

In the general case and for reflections from the bottom the reflection coefficient $\Re(k)$ is not constant and the integral can only be solved approximately or numerically. In order to derive an approximation the of the integral in Equation (24) the Hankel function is expressed in a power series with the first terms giving

$$H_0^1(kr) \approx \sqrt{\frac{2}{\pi kr}} \exp\left[i\left(kr - \frac{\pi}{4}\right)\right] \left[1 + \frac{1}{8ikr} + \dots\right]. \quad (28)$$

This is valid approximation for fields at distances much longer than the wavelength. Restricting the integral of Equation(24) to the first term yields

$$\Phi_{ref}(r, z_r, \omega) = \frac{S(\omega)}{4\pi} \frac{1}{\sqrt{2\pi r}} \int_{-\infty}^{\infty} \Re(k) \frac{\sqrt{k}}{\gamma_1} \exp\left[ikr + i\gamma_1(z_r + z_s)\right] dk. \quad (29)$$

Since the exponential in the integrand will normally be a rapid varying function the value of the integral is expected to be very small except for the values where the phase term of Equation (29) is nearly constant. The phase term of Equation (29) is

$$\alpha = \left(i\gamma_1 |z_r + z_s| + ikr\right) \quad (30)$$

The stationary points are defined as the locations in space were the derivative of the phase with respect to k is equal to zero, the is where $d\alpha/dk=0$. In this

$$r = \frac{(z + z_s)}{\tan(\theta_0)}. \quad (31)$$

These locations of r correspond to the ray indicated in Figure 14. The result is quite simple, the reflected wave field is equal to that of the image source multiplied with the reflection coefficient that at the specular angle.

There are however situations where this approximation is not sufficient in practice and this is discussed by Brekhovskikh and Lysanov (2003) and in the following we use their results without proof. The accuracy of the approximation depends on the source or receiver distance from the bottom interface. The result of the analysis is that the distance z from the bottom must satisfy

$$z \gg \frac{\lambda}{2\pi} \frac{\frac{\rho_b}{\rho_w}}{\sqrt{\left(\frac{c_b}{c_w}\right)^2 - 1}}. \quad (32)$$

With the water parameters of $\rho_w = 1000 \text{ kg/m}^3$ and $c_w = 1500 \text{ m/s}$, and the bottom parameters of $\rho_b = 1500 \text{ kg/m}^3$ and $c_b = 1700 \text{ m/s}$. Equation (32) gives the requirement of $z \gg 0.5 \lambda$. for the validity of using plane wave reflection coefficient at the bottom interface. At a much harder bottom with $\rho_b = 1800 \text{ kg/m}^3$ and $c_b = 3000 \text{ m/s}$, we get that $z \gg 1.0 \lambda$. Hence the condition for validity is somewhat easier to satisfy for a soft bottom than for a hard bottom. The plane wave reflection coefficient result is always valid for the perfectly reflection boundary. Thus it is correct to apply the plane wave reflection coefficient for the sea surface. For the reflection from the bottom the use of plane wave reflection coefficients represents an approximation.

5.2 Caustics and turning points

As mentioned before, the locations where $dr/d\theta_0 = 0$ are called caustics where the ray phase is decreased by 90° and where the intensity, according to ray theory, goes to infinity. In reality the intensity is high, but finite, and the basic ray theory breaks down at these points. There exists theories to amend and repair the defects of ray theory at these points [Officer (1958), Brekhovskikh and Godin (2002), and Jensen et al. (1993)], but such theories are not implemented in the model. PlaneRay only detects the locations of the turning points and caustics, but the accepts the amplitudes as resulting from the numerical evaluation of Equation (11).

Figure 15 shows details of the field at this caustic, with the upper plot showing the rays with initial angles in the range of -6° to -1° and the lower part the geometrical transmission loss calculated numerically from Equation (11). The scenario is the same as in of Figure 1, but for clarity the tracing of rays have been stopped after the first bottom reflection and the figure concentrates on the details the field at the caustic at 1760 m range for a ray with initial angle of -5.6° .

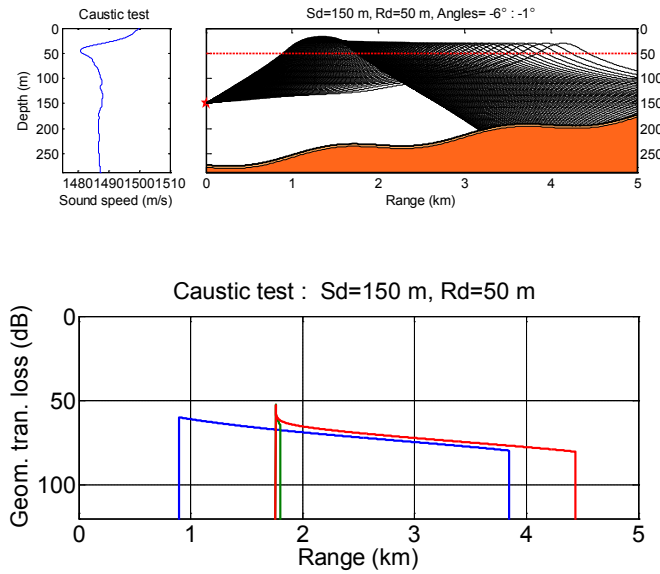


Figure 15 Rays through a caustic (upper) and geometrical transmission loss as function of range (lower)

Figure 16 shows the time response for seven ranges in the interval from 1.6 km to 1.9 km. In this case, the source signal is a Ricker pulse with a peak frequency of 200 Hz. Notice the effect of the 90° phase shift for ranges beyond the caustic at 1760 m and that the amplitude at this range is considerably higher than at the other ranges.

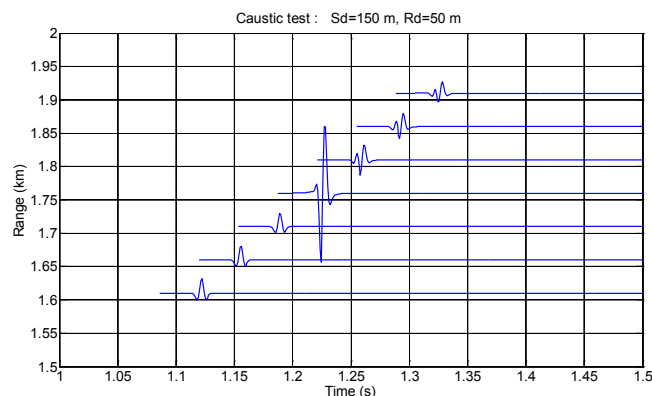


Figure 16 Time responses around the caustic at 1.76 km. The transmitted signal is a Ricker pulse with peak frequency of 200 Hz.

5.3 The principle of reciprocity and its validity in ray modeling

The principle of reciprocity is an important and useful property of linear acoustics and systems theory. Applied to the modeling of wave propagation the principle of reciprocity stipulates that the sound pressure at a position B due to a source at position A is equal to the pressure at A due to an identical source at B . The principle is very general and valid also in cases where the wave undergoes reflections and refraction at boundaries on its path from source to receiver [Landow L. D., and F. M. Lifshitz (1959)].

Figure 17(a) shows a situation where we want to calculate the received field at a fixed observation position B generated by a moving source at position A . Since the PlaneRay model assumes that the source is stationary and the receiver is moving and it may be more convenient to model the reciprocal situation as shown in Figure 17(b) where the bathymetry is flipped and the source and receiver depths are interchanged.

Note that the reciprocity principle is strictly valid for point sources and the direction and that care must be exercised when using directional sources.

We test the reciprocity principle in practice and check its validity in the PlaneRay model. We chose the same scenario as with the source at 150 m depth and emitting a short Ricker pulse with main frequency 50 Hz. The receiver is at 50 m depth in the actual situation [Figure 17(a)], in the reciprocal situation [Figure 17(b)] the source and receiver depths are interchanged. The eigenrays for the two reciprocal situations are shown in Figure 18 where the two ray diagrams show the most significant eigenrays.

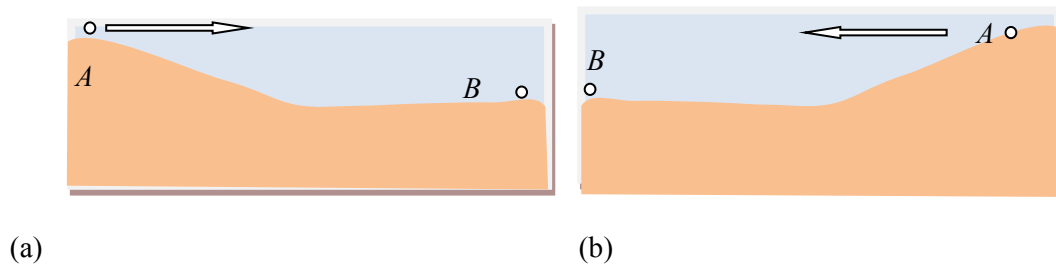


Figure 17 (a) The real situation with a moving source (A) and a stationary observer (B)
 (b) The reciprocal situation with a stationary source (B) and a moving receiver (A).

In this example the bottom is modeled with a 10 m thick sediment layer over a homogenous solid half space. The sedimentary layer has a sound speed of 1700 m/c, attenuation 0.5 dB per wavelength and density of 1500 kg/m³. The solid half space has a compressional sound speed of 2500 m/s, a shear speed of 750 m/s and density is 2500 kg/m³. Both wave types have absorption of 0.5 dB per wavelength.

Figure 19 presents the modeled time response for the two situations. The two results are nearly identical which proves as expected that the reciprocity principle is correctly represented in ray modeling.

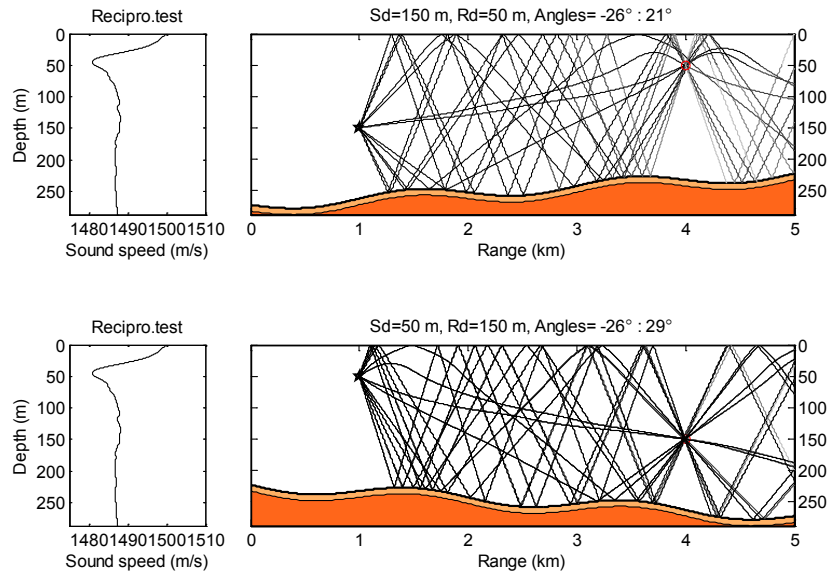


Figure 18 Transmission over an undulating sloping bottom with a northern summer sound speed profile with the eigenrays for the two reciprocal situations.

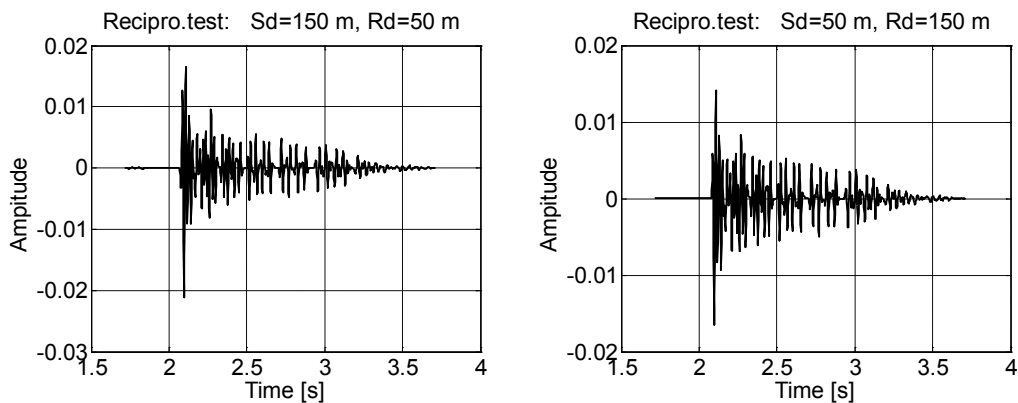


Figure 19 Time signal from a source at position *A* (150 m) to receiver at position *B* (50 m) compared with the reciprocal situation with transmission from *B* to *A*.

The reciprocity principle may be used for checking the validity of the modeled result. It is a good indication that the model result is correct if the real and the reciprocal situation this give the same result.

Finally, it should be noted that the reciprocity principle applies to a point-to-point situation. This means that, for instance, that the development of the transmission loss as function source-receiver separation is not the same for the two situations. This is illustrated in Figure 20 where transmission loss as function of source and receiver separation. The two figures are different, as they should be since the bathymetries are not the same. The two transmission losses are only identical at 4 km separation where the two situations are reciprocal.

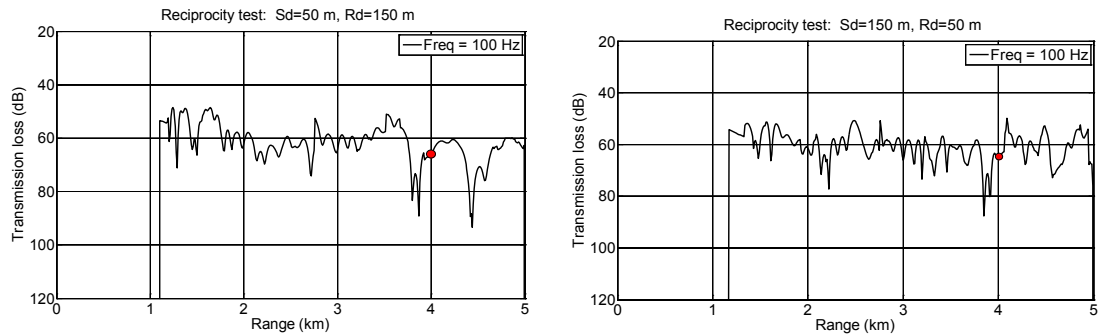


Figure 20 Transmission loss as function of distance for a source at position *A* to receiver at position *B*, compared with the reciprocal situation with transmission from *B* to *A*. The transmission loss at a separation of 4 km are identical is indicated with circles.

6 High frequency applications

PlaneRay was originally intended for low frequency application and most of the applications and comments in this paper reflect the emphasis on such applications. However, there is nothing in the model to prevent its use at any frequency, but there may be a practical problem with aliasing errors in the Fourier transformation to time domain. With a high sampling frequency the required block length of the Fourier transform may be very large with resulting in long computation time and in practice the use of the model may be restricted to relatively short ranges. Alternatively the model allows for specification of a carrier frequency. This carrier frequency is only used to determine the attenuation in the transmission loss calculation using the results of Figure 4. The pulse shape is the short Ricker transient or any other pulse as specified by the user.

7 Accuracy considerations

The accuracy of the PlaneRay model depends on the validity and limitation of ray theory, with the assumption that the reflection from the boundaries, in particular the interactions with the bottom, can adequately be represented by plane wave reflection coefficient. In this section we test these assumptions by comparing with results obtained by the OASES model. Other tests and comparisons can be found in Smedsrud and Tollefsen (2007) and Hovem (2007, 2008).

7.1 Pekeris' waveguide

We present results calculated by PlaneRay model and compare with the results of the wave number integration model OASES [4] for range independent cases with different bottom properties. These cases have been selected because the OASES model is generally accepted to be accurate in these cases. Thus the comparison is relevant for assessment of the accuracy of ray theory and the use of plane-wave reflection coefficients in representation of the bottom interaction.

Four cases are considered, all with constant sound speed (1500 m/s) and constant density (1000kg/m^3) in the water column. The other parameters are given in Table 2.

Table 2 Bottom parameters for four different cases of Pekeris' waveguide.

Case	Pekeris-1	Pekeris-2	Pekeris-3	Pekeris-4
c_{p1} [m/s]	1700	3000	1700	1700
c_{p2} [m/s]	1700	3000	3000	4700
c_{s2} [m/s]	0	0	500	2200
ρ_1 [kg/m ³]	1500	1800	1800	1500
ρ_2 [kg/m ³]	1500	1800	1800	2500
α_{p1} [dB/ λ]	0.5	0.5	0.5	0.5
α_{p2} [dB/ λ]	0.5	0.5	0.5	0.5
α_{s2} [dB/ λ]	0	0.5	0.5	0.5
Layer thickness [m]	0	0	5	5

In the first case, Pekeris-1, the bottom is modeled as a homogenous fluid with a sound speed of 1700 m/s, density of 1500 kg/m³, and absorption of 0.5 dB/wavelength. Figure 21 shows the transmission loss as function of range and frequency and the time response, (as function of reduced time) at a number of receivers out to the range of 20 km. The dashed red line corresponds to rays striking the bottom with the critical angle and the expression for this line is

$$t_{red} = \frac{r}{c_0} \left(\frac{1}{\cos \theta_{crit}} - 1 \right) = r \left(\frac{c_b - c_0}{c_0^2} \right). \quad (33)$$

Rays that propagate at angles closer to the horizontal plane than the critical angle experience almost no bottom reflection loss and may therefore propagate to long distances. Rays with steeper angles will experience higher reflection losses and die out quite rapidly with range. Thus the time duration of the impulse is directly determined by the ratio of sound speeds in the water and the bottom. This estimate of the time duration of the channel impulse response is assumes that the bottom is fluid homogenous and flat but the estimate may also be useful in other cases with moderately range dependent depth and with solid or layered bottom.

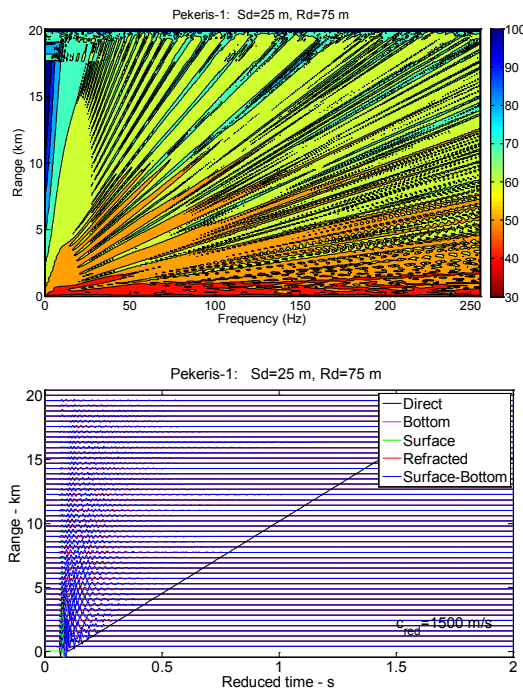


Figure 21 Frequency and time response of a Pekeris' wave guide where the bottom sound speed is 1700 m/s, the density is 1500 kg/m³ and the attenuation is 0.5 dB/wavelength. Upper: Transmission loss as function of range and frequency. Lower: Time response at receivers with distances from 100 meter to 20 km from the source. The source signal is a short transient (Ricker wavelet).

We use this example to comment on an issue that is often discussed, namely whether the transmission loss follows the rule of spherical ($20 \log(r)$) or cylindrical ($10 \log(r)$) spreading. Figure 22 shows the peak and rms pressure plotted as function of distance from the source. The data is extracted from the time responses shown in Figure 21. Figure 22 shows that the peak pressure decays at the rate of spherical spreading whereas the rms pressure follows the cylindrical spreading. In addition there is the effect of acoustic absorption.

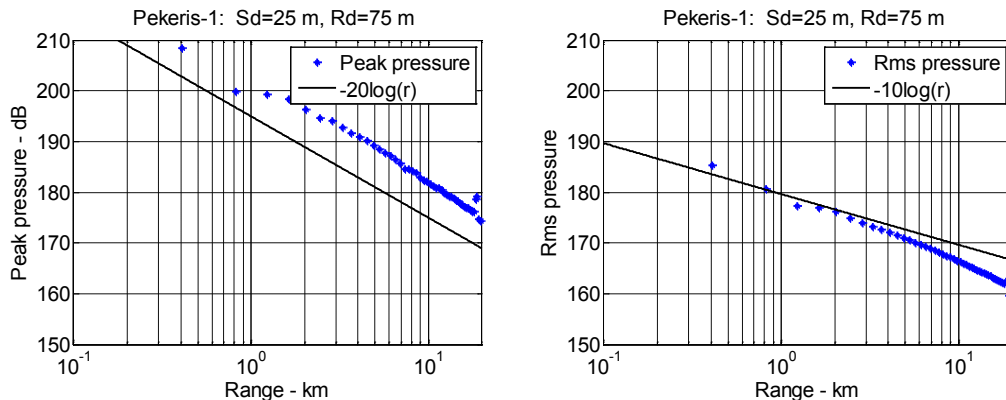


Figure 22 Plots of peak pressure and rms pressure for the received waves in the Pekeris-100m waveguide shown in Figure 21

Figure 23 shows transmission loss as function of range for the selected frequencies of 25 Hz, 50 Hz, 100 Hz and 200 Hz, compared with the results of OASES. For the lowest frequency the agreement is rather poor, but for the higher frequencies the PlaneRay results agree quite well the OASES results. The oscillations in transmission loss with range can be explained by mode interference.

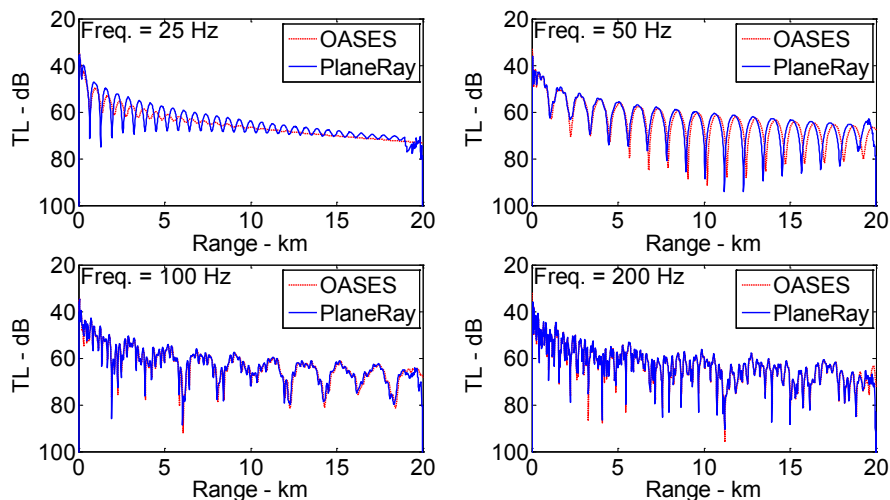


Figure 23 Comparison of the transmission loss as function of range for different frequencies by PlaneRay (solid red line) and OASES (dotted blue line) for Pekeris' wave guide where the bottom sound speed is 1700 m/s, the density is 1500 kg/m³ and the attenuation is 0.5 dB/wavelength.

Notice that the interference patterns of the two results are shifted in phase, most pronounced for low frequencies and long ranges. This shift indicates general a limitation of ray theory. The generally accepted range of validity of ray theory is that the frequency must be higher that the frequency where the water depth is 2-4 times the acoustic wavelength. Applied to our case this means that frequency must be higher than 30 Hz to 60 Hz for ray theory to be an acceptable approximation. This agrees well with the results of Figure 23.

7.2 Elastic homogenous bottom

Consider the same scenario, but with the bottom modeled as an elastic half-space with compressional sound speed of 3000 m/s, shear speed 500 m/s, and density 1800 kg /m³, both waves with attenuations of 0.5 dB/wavelength. This gives the reflection loss displayed in Figure 24 as function of angle and frequency. In his case the critical angle, determined by the compressional speed of 3000 m/s, is about 60°. The reflection loss at lower angles is caused by wave attenuation and shear wave conversion in the bottom.

Figure 25 shows the time response. Note that the time responses are much longer in this case with a high speed bottom than for the low speed bottom (see Figure 21). Consequently the length of the time

window T_{\max} must be increased in order to reduce aliasing errors and to accommodate the longer channel impulse. The higher critical angle about 60° requires also that the span of initial angles much be increased accordingly.

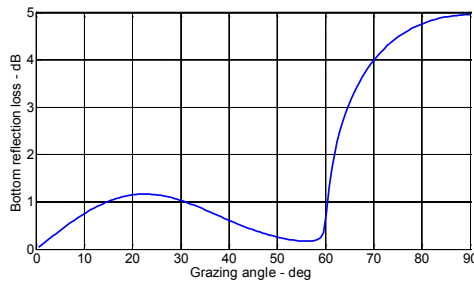


Figure 24 Bottom reflection loss for a homogeneous solid bottom with $c_p=3000$ m/s, $c_s=500$ m/s and $\rho=1800$ kg/m³.

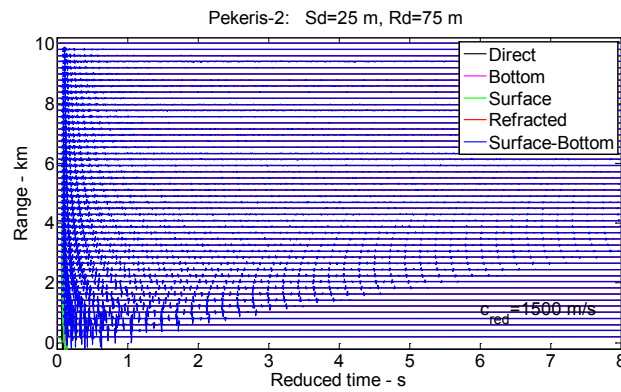


Figure 25 Time response for at receivers with distances from 100 meter to 20 km from the source for a 100 m deep water channel with a homogeneous bottom with compressional sound speed of 3000 m/s, shear speed 500 m/s, density of 1800 kg/m³ and the attenuation is 0.5 dB/wavelength.

Figure 26 shows the transmission loss as function of range for the frequencies of 25 Hz, 50 Hz, 100 Hz, and 200 Hz, compared with the results produced by the OASES model.

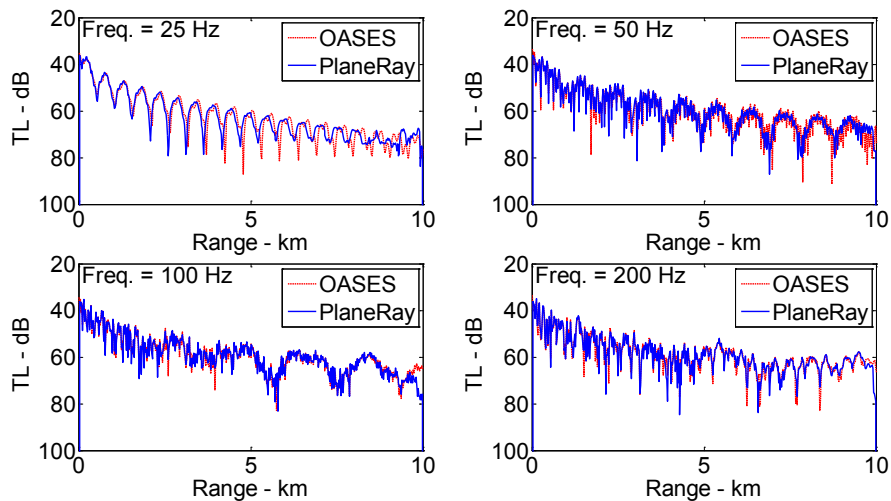


Figure 26 Comparison of the transmission loss as function of range for selected frequencies by PlaneRay (solid blue line) and OASES (dotted red line) for Pekeris' waveguide with a homogenous solid bottom with compressional wave speed of 3000 m/s and shear wave speed 500 m/s. Both wave attenuations have the values of 0.5 dB/wavelength.

7.3 Distance from borders

Section 5 discussed the validity of using plane wave reflection coefficients to represent the interaction with the bottom, with the conclusion that the source and receiver need to be at least at a wavelength distance from the interfaces. In this section we compare the transmission loss calculated with PlaneRay and the OASES mode for different frequencies. Figure 27 shows the result using the parameters of a soft bottom and Figure 28 shows the results for a hard bottom. In both cases the receiver is at 95 m depth, which is 5 m above the seabed. Both examples show that the comparisons with the OASES results are somewhat poorer for the frequency of 25 Hz, but quite good for the higher frequencies.

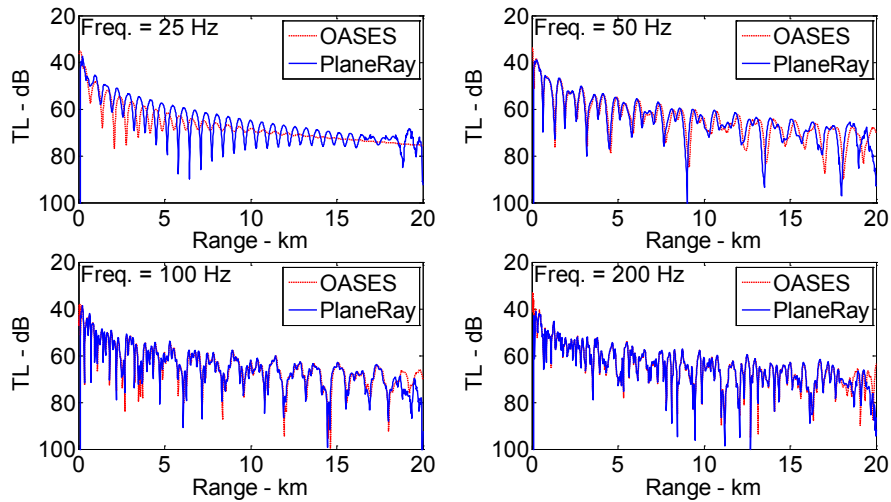


Figure 27 Pekeris -1 with source at 25m depth and receiver at 5 m above the seabed

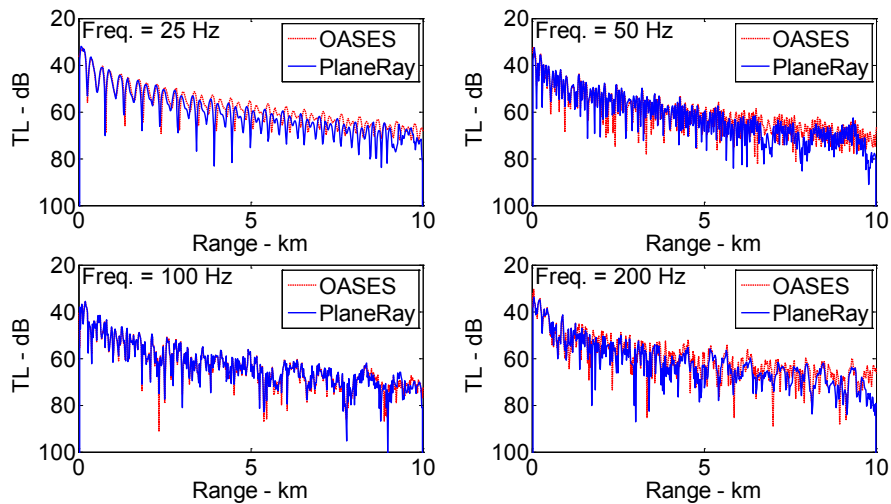


Figure 28 Pekeris -2 with source at 25 m depth and receiver at 5 m above the seabed

7.4 Layered bottom

Since the effect of the bottom is modeled by plane wave reflection coefficient, it is interesting to compare the PlaneRay results with a model that treats a layered bottom correctly. Consider the case of a bottom with a sediment layer over a half-space hard bedrock. The water depth is 100 m, the thickness of the sediment layer is $D = 5$ m with sound speed and density of the sediment layer of 1700 m/s and 1500 kg/m^3 respectively. In the first of the layered cases, Pekeris-3, the compressional sound speed in the elastic half space is 3000 m/s, the shear speed is 500 m/s, both with attenuations 0.5 dB/wavelength, and the density is 1800 kg/m^3 . This gives a bottom reflection loss shown in the left-hand plot in Figure 6.

Figure 29 shows the time response and the transmission loss results and Figure 26 shows the comparison with the OASES results. As before the agreement is good except for the lowest frequency.

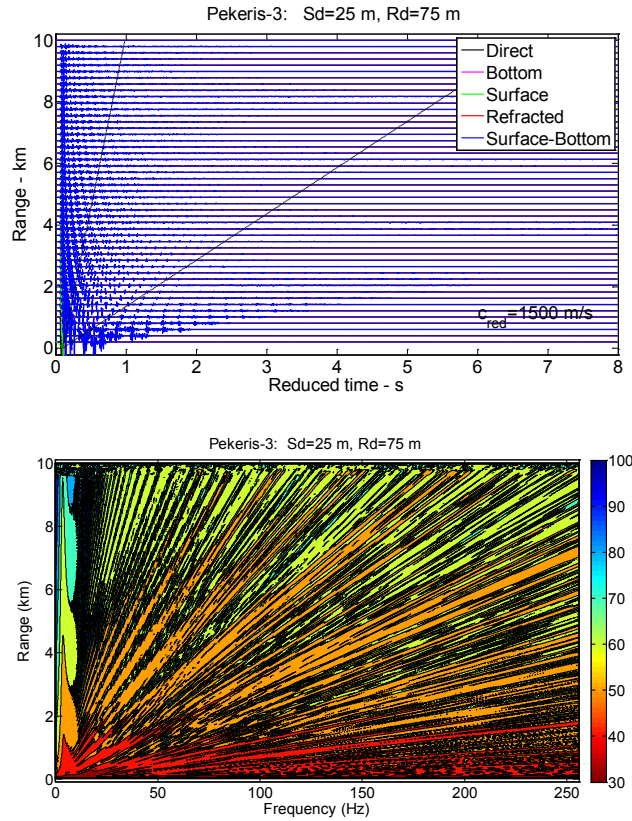


Figure 29 Time responses as function of range (upper), and transmission loss as function of range and frequency (lower). Sediment layer with thickness 5 meter over an elastic half space with compressional speed 3000 m/s, shear speed 500 m/s.

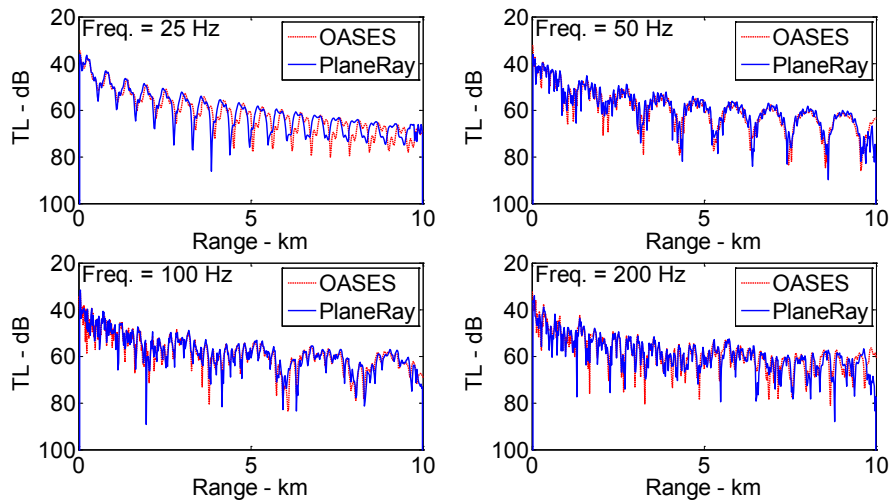


Figure 30 Comparison of the transmission loss as function of range for different frequencies by PlaneRay (solid red line) and OASES (dotted blue line) for Pekeris' waveguide with a layered bottom where the elastic half space has a compressional wave speed of 3000 m/s and shear wave speed 500 m/s. Both wave attenuations have the values of 0.5 dB/wavelength.

In the second layered case, Pekeris 4, the elastic half-space is hard bedrock with compressional speed of 4700 m/s and shear speed 2200 m/s with density of 2500 kg/m³. The sediment layer has the same parameters as in the previous case. This results in the bottom reflection loss, depicted at the left of Figure 6, with an anomalous high loss at low incident grazing angles and low frequencies.

Figure 31 shows the time and frequency domains manifestations of these high bottom reflection losses. Here, the upper graph shows the time response for a number of ranges up to 10 km and the lower graph shows the transmission loss as function of range and frequency.

The straight lines in time plots of Figure 31 correspond to grazing incident angles of 5°, 28° and 47°. Recall from Figure 6 that the 47° is the shear critical angle of the elastic half space, 28° is the critical angle of the sediment sound speed; and 5° is the angle for significant increases bottom reflection loss at low frequencies. This figure shows a triangle-shaped plateau of high reflection loss at angles lower than 20° with two peaks at 80 Hz and 200 Hz. This high reflection loss may occur for certain combinations of bottom parameter values and can be attributed to the excitation of an interface wave at the boundary between the sediment layer and the solid half space. This has previously been discussed by Hovem and Kristensen (1992), Tollefsen (1998) and by Ainslie (2003) and will not be discussed further here.

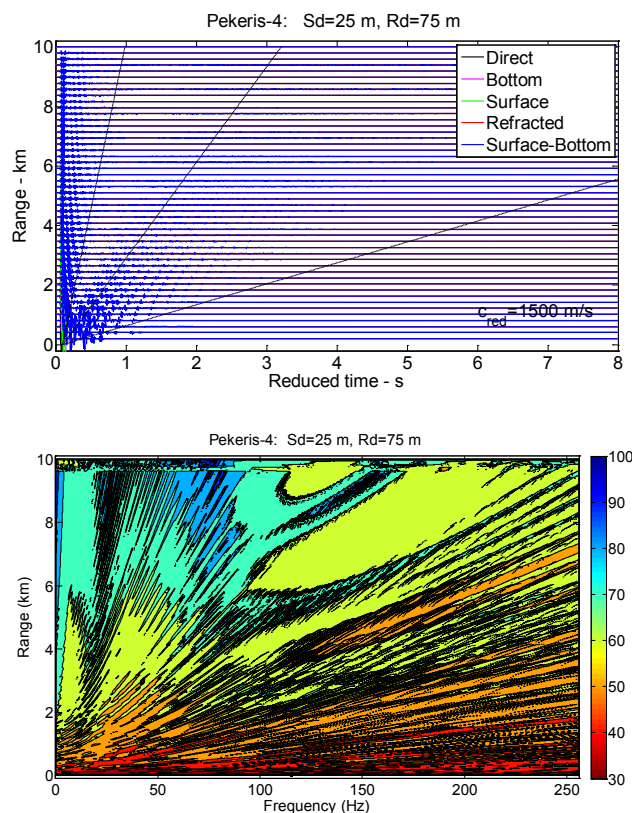


Figure 31 Time responses as function of range (upper), and transmission loss as function of range and frequency (lower). Sediment layer with thickness 5 meter over an elastic half space with compressional speed 4700 m/s, shear speed 2200 m/s.

This angle-frequency dependence of the bottom reflection losses results in strongly reduced amplitudes of the arrivals between the two lines of 5° and 28° as shown in Figure 31. At angles higher than 28° and lower than 47° , the shear speed critical angle, the amplitudes are higher as a consequence of lower reflection losses in the region.

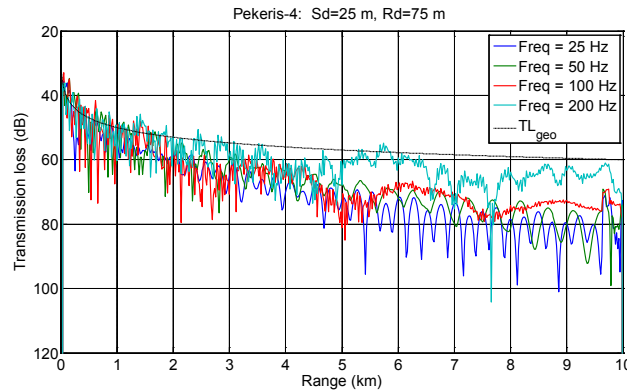


Figure 32 Transmission loss as function of range and for the frequencies of 25 Hz, 50 Hz, 100 Hz and 200 Hz. Sediment layer with thickness 5 meter over hard bedrock with shear speed 2200 m/s.

Figure 33 shows the transmission loss as function of range for the selected frequencies of 25, 50, 100 and 200 Hz. The results of the Plane Ray model are compared with the OASES results. The agreements are quite good for the higher frequencies, but poorer at lower frequencies, as seen before. Notice that both OASES and PlaneRay predict significantly higher transmission loss for frequencies lower than for 200 Hz.

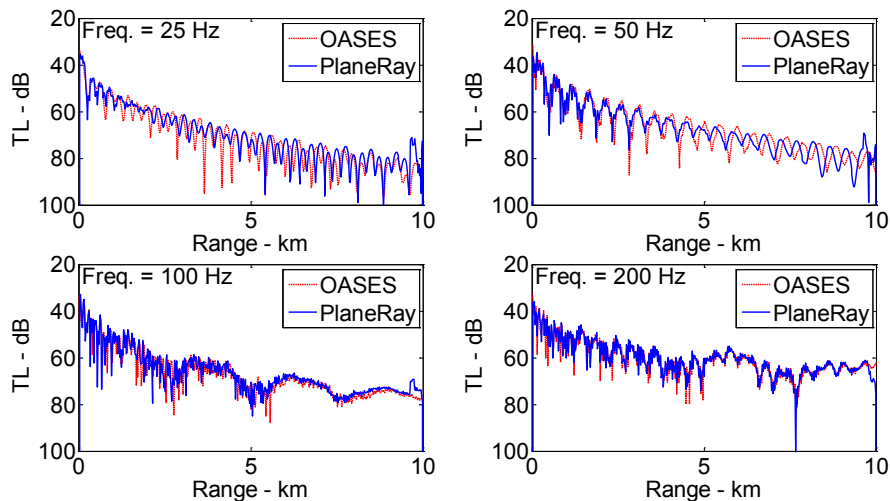


Figure 33 Comparison of the transmission loss as function of range for the frequencies of 25, 50, 100 and 200 Hz. By PlaneRay (solid red line) and OASES (dotted blue line). The water depth is 100 m, the sound speed is constant 1500 m/s and the bottom has a 5 meter sediment layer over a hard-rock half-space with shear speed of 2200 m/s.

8 Producing results as function of depth

The calculation in PlaneRay is organized with fixed steps in depth and variable increments in range. Therefore, the natural output is as function of range for fixed source and receiver depths. However, there are many applications where it is desired to determine the sound field as function of depth for fixed distances for example when using a vertical receiving array. To obtain relevant results for such situations the user need to set up a loop for repeating the ray trace calculation at the required receiver depths and store the intermediate result.

The calculation of sound fields as function of depth is illustrated in the example of Figure 34, where a vertical array is suspended from the surface at two km distance from the source. The array has 10 hydrophone phones spanning the depth from 10 m to 100 m. The time response at the distance of 2 km is calculate independently for each of the 10 hydrophone and stored. Figure 35 displays the accumulated results showing the time responses at the depths of the 10 hydrophones.

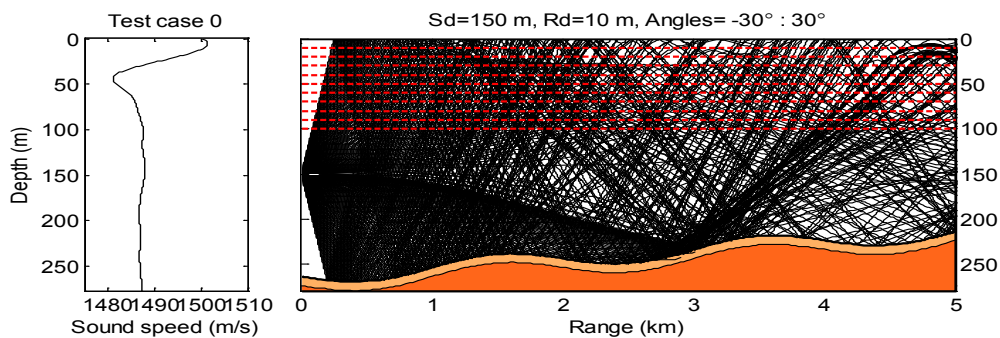


Figure 34 The vertical array located at a distance 2 km from the source with 10 hydrophones spans the depth from 10 m to 100. The sound speed and bathymetry is the same as in Figure 1.

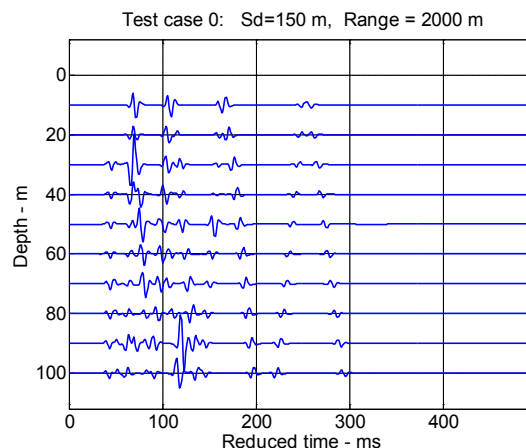


Figure 35 Received time signals as function of receiver depth for the distance of 3000 m from a source at 50 m depth. The sound speed and bathymetry is the same as in Figure 1.

The next example considers the case of a source close to the bottom at 150 m depth transmitting to a receiving array suspended from the surface and covering the depth interval from 8 m to 16 m. Figure 36 shows the dominating eigenrays to the deepest hydrophone at 16 m and Figure 37 shows the received signals to the eight hydrophones on the array at distance of 2 km from the source. Note that in this case the first arrivals seem to be coherent over the depth interval covered by the array.

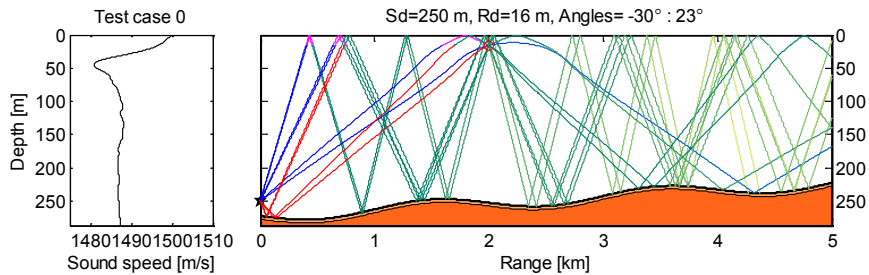


Figure 36 Eigenrays from a source at 150 m depth to a receiver at 2 km distance and 16 m depth. The sound speed and bathymetry is the same as in Figure 1.

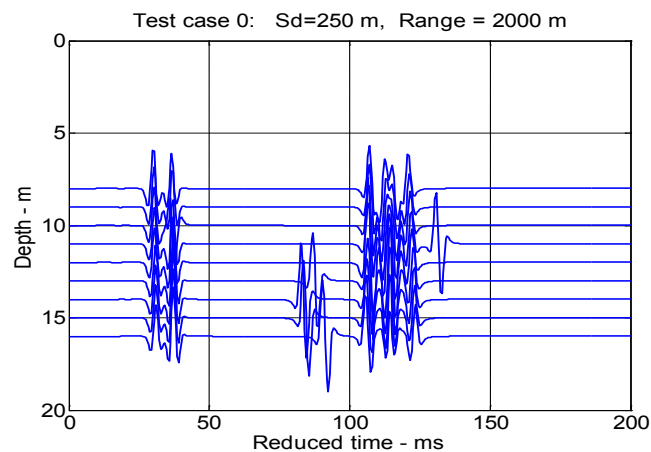


Figure 37 Received time signals as function of receiver depth for the distance of 2000 m from a source at 250 m depth. The sound speed and bathymetry is the same shown in Figure 1

These examples demonstrate that the PlaneRay model with the depth extension is useful for studying the structure of signals received at vertical arrays. However, this requires more computation time since the ray trace calculations are done independently for each receiver depths.

9 Conclusions

The PlaneRay model is an acoustic propagation model intended for use in moderate range dependent environments, particularly in situations where the structure and material properties of the bottom vary with range. The complete acoustic fields are calculated by coherent addition of the contributions of a large number of eigenrays. No rays are traced into the bottom, but the bottom interaction is modeled by local plane wave reflection coefficients. The bottom can be a fluid-like sedimentary layer over an elastic half space and the layer thickness, the sound speeds and the densities can vary with range. The sound speed of the water may vary with depth, but not with range.

Ray tracing calculation is, by definition, frequency independent and therefore the calculations of ray trajectories through the water column are not dependent on frequency. Frequency dependency is introduced separately afterwards with the bottom or surface reflection coefficient, by layering and absorption, or by diffuse scattering of rough ocean surface or bottom interface. Therefore the ray tracing and the determination of the eigenrays need to be done only once for each scenario, i.e. for a fixed bottom topography, sound speed profile and source and receiver depths. Since these calculations are the most computational intensive parts of the code, the model is quite efficient for broad frequency band calculations and consequently for the calculation of time responses.

Ray tracing is high-frequency approximation to the solution of the wave equation and therefore the accuracy and validity at lower frequencies may be questioned, in particular the use of plane ray reflection coefficient to represent the bottom effects. This problem has been considered both theoretically and by simulations and comparison with more accurate model. The results of this study shows that source and receiver should be at a height above the bottom of at least half a wavelength, but there is no similar requirement to the distance from the sea surface. Another, and less fundamental limitation, is the numerical accuracy of the determination of the eigenrays, which is most serious in the calculation of the ray amplitude or the transmission loss. These inaccuracies are of more practical nature and can be reduced by refinements in the calculations.

The main conclusion is that ray tracing modeling may be a quite useful technique for applications moderately range dependent environments and, as such be a valuable addition and alternative to other models with different advantages and limitations.

References

Abrahamsson, L. *RAYLAB---a ray tracing program in underwater acoustics*, Sci. Rep. FOIR--1047--SE, Division of Systems Technology, Swedish Defence Research Agency, Stockholm, Sweden, (2003).

Ainslie A. M., *Conditions for the excitation of interface waves in a thin unconsolidated sediment layer*, J. Sound and Vibration, 268, pp. 249-267 (2003)

Brekhovskikh, L. M., and Yu. Lysanov. *Fundamentals of ocean acoustics*, 3rd ed. Springer-Verlag, New York City, (2003).

Collins M. D., *A split-step Pade solution for parabolic equation method*, J. Acoust. Soc. Am. 93, pp. 1726-1742 (1993).

Hovem J. M. and Å. Kristensen, *Reflection loss at a bottom with a fluid sediment layer over a hard solid half-space*, J. Acoust. Soc. Am. 92(1), pp. 335-340 (1992)

Hovem Jens M., *PlaneRay: An acoustic underwater propagation model based on ray tracing and plane wave reflection coefficients*, in Theoretical and Computational Acoustics 2007, Edited by Michael Taroudakis and Panagiotis Papadakis, Published by the University of Crete, Greece, pp. 273-289, (2008). (ISBN: 978-960-89785-4-2).

Hovem, J. M. and Knobles, D. P., *A range dependent propagation model based on a combination of ray theory and plane wave reflection coefficient*. Tenth International Congress on Sound and Vibration, 7-10 July, (2003), Stockholm, Sweden

Hovem, J., M. and Knobles, D. P., *A range-dependent propagation model based on a combination of ray theory and plane-wave reflection coefficients*, J. Acoust. Soc. Am. 112, pp. 2393 (2002)

Hovem, Jens M., Hefeng Dong and Xiukun Li. *A forward model for geoacoustic inversion based on ray tracing and plane wave reflection coefficients*, Proceedings of the "Acoustic Inversion Methods and Experiments for Assessment of the Shallow Water Environment", Ischia, "2nd workshop, 28 30 June, (2004), Ischia, Italy.

Hovem, Jens M., *PlaneRay, An acoustic underwater propagation model based on ray tracing and plane-wave reflection coefficients*. FFI-rapport 08/00610, 10.03.2008. Forsvarets forskningsinstitutt/Norwegian Defence Research Establishment.(2008)

Ivansson,S., *Stochastic ray-trace computations of transmission loss and reverberation in 3-D range-dependent environments*, ECUA 2006, Carvoeiro, Portugal, pp. 131-136.(2006).

Jensen F. B., W. A. Kuperman, M. B. Porter, and H. Schmidt, *Computational Acoustics*, AIP Press, New York Jersey, (1993).

Jensen F. B. and M. C. Ferla, *SNAP: The SACLANTEN normal-mode acoustic propagation model*, SM-121, SACLANT Undersea Research Centre, La Spezia, Italy (1979).

Officer, C. B. *Introduction to the theory of sound transmission*. McGraw-Hill, New York City, (1958)

Porter, M. B., *The Kraken normal mode program*. Rep.SM-245. SACLANT Undersea Research Centre, (Nato Undersea Research Centre), La Spezia, Italy, (1991).

Porter, M. B., and E. L. Reiss, *A numerical method for ocean acoustic normal modes*. J. Acoust. Soc. Am. 76, pp. 244-252 (1984).

Schmidt H., *SAFARI: Seismo-acoustic fast field algorithm for range independent environments*. User's guide, SR-113, SACLANT Undersea Research Centre, La Spezia, Italy (1987).

Smedsrud, M., and Tollefsen, D., *Test of the PlaneRay propagation model for selected low-frequency scenarios*, FFI report 2007/00921, Norwegian Defence Research Establishment, Kjeller, Norway, (2007).

Svensson, E and I., *Estimation of acoustic parameters of a shallow-water communication channel*. ECUA 2006, Carvoeiro, Portugal, pp. 69-74. (2006).

Tollefsen, Dag, *Thin-sediment shear induced effects on low frequency broadband propagation in a shallow continental sea*, J. Acoust. Soc. **104**(5), pp. 2718-2726, (1998).

Westwood, E. K and C. T. Tindle, *Shallow water time simulation using ray theory*, J. Acoust. Soc. Am. **81**, pp. 1752 -1761 (1987).

Westwood, E. K and P. J. Vidmar, *Eigenray finding and time series simulation in a layered-bottom ocean*, J. Acoust. Soc. Am. **81**, pp. 912-924 (1987).

A.1 Short users guide to PlaneRay

A.1.1 General

PlaneRay is a tool box and users need to have a good understanding of ray theory and underwater acoustic propagation. The input parameters need to be specified consistently with the theory and limitations of ray theory. The program does not check the input parameters and if anything is wrong the program may crash without warnings. The core is the calculation of ray trajectories based on the inputted sound speed profile, the bathymetry and the source position. It is the responsibility of the user to provide correct input information. Here are some points to observe:

The sound speed profile must contain values for all depths. The program will crash without warnings if a ray reaches a deeper depth than covered in the sound speed profile. If the sound speed profile is taken from a CTD record, remember that CTD recordings often end at a depth where the operator has decided that the temperature and the salinity have reached constant values. In such cases you need to extrapolate the sound speed profile all the way to the bottom. For instance by calculating the sound speed gradient of the deeper measurements and add sound speed values using linear extrapolation.

PlaneRay interpolates the input sound speed profile to equal spaced depth intervals (specified by the user in the input file). The interpolation routine in MatLab requires that the depth values are monotonically increasing or decreasing. Sometimes this is not true because the CTD instruments have been moving up and down during lowering or recovery. The user has to filter out these variations before submitting to the program.

The user can specify the method of interpolation by setting the parameter `sspmethod` to for instance 'linear' or 'spline'. If the inputted sound speed profile is sparse, the interpolation, especially the spline interpolation, may create unrealistic values. It is a good practice to check the interpolated profile before starting the calculations. What is said about the sound profile also applied to the bathymetry, here the parameter `bathymethod` determines the interpolation method.

The code is written in Matlab, which is great in terms for flexibility to specific user needs. In terms of running time it is not so great. The program will for many appear to be quite slow, but here are some guidelines for considerations.

The running time for steep rays may be significantly longer than near horizontal rays for reaching a given range. Again, be modest in the first run by .

The time plots are derived by Fourier transformation of the product of the source function and the transfer function. The user has to specify the sampling frequency and the FFT block length. It is the user responsibility to select these parameters such that serious time does not result. If you require long ranges and many receiver phone positions you may need long FFT block length requiring significant computer time.

I have spent "lots of time" developing the PlaneRay program and have finally decided to release the program for free use. I hope that you respect my intellectual rights by acknowledgement and reference to this document. If you find errors, and for certain there are errors, send me email with remarks and suggested corrections and I will update the code accordingly.

Good luck!

A.1.2 How to run the program

This is a commented version of the driver program to run PlaneRay. Take away the comments in the box, keeping only the highlighted items and store it under the name planeray.m. Execute the file by writing: planeray

The calculations start by calling the program planeray, which calls all relevant PlaneRay programs. This includes the program planerayinput, which sets up the environmental parameters and the parameters for the calculations. This information is the struct files env. and para. , which are stored for other use. The content of these two files are displayed on the screen. You should control the scenario specified by env and para is what you want

```
close all;
all;clc;
Example=input( 'Example ? ');
rawinput = planerayinput(Example);
[env, para] = initpara(rawinput);
save env; save para;
disp('Environmental parameters');disp(env);
disp('Run parameters'); disp(para);
disp(' Is this what you want, press any key to continue')
pause
```

The calculations of the ray trajectories start by calling the program tracerays with arguments env and para. The program is sorting and interpolating the ray history producing the eigenangles and other variables need in the calculation of the wave of the wave field.

```
[EIG, COUNT, SUFBOT, Rays] = tracerays(env, para);
[eigenangle, EIG, COUNT, SUFBOT, Rays, para]=.....
plotrays(EIG, COUNT, SUFBOT, Rays, env, para)
```

The frequency transfer function is calculated by the program transfunc. The result is obtained by coherent addition of all eigenray contributions and includes the standard seawater attenuation for the actual frequencies. This function is used both for determination of the transmission loss as function of range and frequency (origin==1) and for the calculation of the time responses (origin==2), which depend of the source signal and directivity.

```
[transfer_function,trans,c_red,eigen] = transfunc(EIG, COUNT,
SUFBOT,env, para,origin);
```

The program `transloss` produces the transmission losses values as function of range, and for frequencies specified in the input and stored in parameter file. The results are plotted when `para.tlplot==1`. The plots are in different formats numbered from 10 to 12

```
para.tlplot==1
```

```
TL=transloss(EIG, COUNT, SUFBOT, env, para);
```

To obtain the time domain results the user need to specify the source signal. This specification must be included in the function `getsourcesignal(source_type,para)`. The default source signal, obtained by setting `source_type=1`, is a Ricker pulse with a center frequency fixed to 10% of the sampling frequency contained in `para.fs` and defined in the input file. Other source signals can be implemented by the user. The output `t_start` is a convenient starting time of the pulse

```
[source_signal, t_start] = getsourcesignal(type,para);
```

The time responses for the ranges specified in `para.range_phone`; are produced by calling `[signal, h, eigen]=timeresponse(EIG, COUNT, SUFBOT, env, para, source_signal, t_start)`. In the current version only the "signal" result is used. The received signals are plotted in various forms as function of both real and reduced times by calling `plot_time_signals`. The time plots are numbered from 20 to 24

```
if para.timeplot==1; plot_time_signals; end;
```

Auxiliary programs

The programs defined above are the programs normally used for production of results. In addition the PlaneRay package contains a number of other programs that may be useful for error control and to obtain a better understanding of the wave field and how the program works

The program `ploteigstructure` produces plots of range to receiver array as function of initial angle, and geometrical spreading loss as function of range for each ray class. Make sure that you understand the results before continuing.

```
if para.diagnostics==1; ploteigstructure(Rays, EIG, COUNT, env, para);end;
```

The eigenrays are found by linear interpolation of range vs initial angle [see figure (10) resulting from `ploteigstructure`] and in most cases this gives sufficient accuracy. This version of PlaneRay also contains a more an iterative algorithm to find the eigenrays more accurately. The number of iterations is controlled by `para.N_iterations` and by the error limit (m) specified in `para.eig` precision. The function `findeigenray` finds the eigenray angles and calculates and plots the trajectories of the eigenrays

The eigenangles are saved in the file `eigen_angles` and it is up to the user to make use of the results; for instance by including `eigen_angles` in the set of initial angels specified in `planeray` input program

Example:

```
para.searcheigenray=1;
para.N_iterations=3; para.eigprecision=1;
if para.eigplot==1;
    eigrange=para.eigrange;% The ranges for which you want to find the eigenrays
    N_ranges=length(eigrange);
    N_angles=20; % Estimate of the maximum number of eigenrays;
    eigen_angles=zeros(N_ranges, N_angles);
    for n=1:N_ranges;
        para.eigrange=eigrange(n);
        ang=findeigenray(eigenangle,env,para,EIG.count);
        eigen_angles(n,1:length(ang))= ang;
    end
end;
save eigen_angles;
```

The source directivity is generated by automatically user by the function `getbeamspec(para,initial_angle, arrayno)`. This function introduces the appropriate directivity weighting for every initial launch angle at the source in the transfer function and thereby in the time signals, not in the transmission loss.

With `arrayno==1` the directivity is that of a linear vertical array with N_e elements and spacing Δx as specified in `planerayinput`. $N_e=1$ yields the omnidirectional beam pattern.

The beam patterns for the frequencies contained `para.frequencies` are displayed in figure (51) by calling

plot_beamspectrum

Plots in figure (50) the directivity of the source as specified in `planerayinput`

plot_source_signal(source_signal, para)

In case you want to generate your own plots you can use the program `post_processing`. This program loads the results of the last `PlaneRay` calculations such as the transmission losses, the time responses and the files `env` and `para`. Thereby you don't have to redo the calculation just to change the output format. This facility also enables the user to compare run with different parameters.

post_processing

`PlaneRay` is organized such that the results come out as function range for a for a fixed source location and fixed receiver depths. In many cases the user may want to compute the field as function of depth at a fixed range. For such use is required that `PlaneRay` is run repeatedly for each receiver range, which may take some time.

To calculate field as function of depth use the program `TimeDepth_plots`.

This program works in the same way as `planeray` and requires the same input information specified in `planeray` input. Furthermore, `TimeDepth_plots` will ask for the range (one) and the string of the depths you want calculate.

It is recommended that you first run `planeray` to make sure that everything works out as intended.

A.1.3 The input file

```
%% planerayinput.m
%% Author: Jens M. Hovem
%% Copyright 2011 Acoustic Research Center, NTNU
%% Revised Date: 2011/01/11
%% This program sets the parameters most likely to be used.
%% The settings can be overruled by statements below to suit your case.

%% Note that the parameters searchrays and beamdisp are not activated in
%% this version of PlaneRay

function rawinput = planerayinput(Example)
PLR_initial_settings;

switch Example;

    case 0
        title_tekst='Test case 0';
        %% Give a title to the case you are running

        %% *****Sound speed profile*****
        %% Specify the sound speed profile (ssp) in any way you want,
        %% but end up assigned values for c_input and z_input; In this
        %% example the ssp is contained in the store file ssp_case_0.mat
        %% The ssp will later be interpolated to equal depth spacings of
        %% del_z. Normally del_z is selected to be less than one hundred
        %% of the maximum water depth.
load ssp_case_0; ssp=ssp_case_0;
c_input=ssp(:,1); z_input=ssp(:,2); del_z=.2;

        %% Special ray tracing algorithm for constant sound speed
        %% The reduction speed c_red is selected to produce plots of time
        %% responses as function of reduced time.
        %% A convenient choice is in this case is
c_red=1480;
        %% *****Geometry*****
R_max=6000; % Maximum range in meter for ray calculations
N=50000; % Max number of calculated points per ray
z_source=25; % Source depth in meter
z_receiver=100; % Receiver depths in meter
range_source=0; % Range position of the source
eigplot=1;eigrange=[3000];
        %% This parameter is only used to produce plots of eigen rays to
        %% the ranges contained in the vector eigrange.

        %% *****Bottom topography*****
        %% Bottom topography is described with the range R_b where the
        %% depth is Z_b. The user has to write, load or otherwise
        %% generate the range depth-coordinates.
        %% This is an example of gently upward or downward rolling hill
        %% depending on the value of flip
flip=0;
R_b=0:1: R_max; z_max=max(z_input);
```

```
Z_b=0.95*z_max-R_b*0.010+ 10*sin(pi*(5*R_b/R_max));
if flip==1
Z_b= fliplr(Z_b);
z_r=z_receiver; z_s=z_source;
z_receiver=z_s; z_source=z_r;
end;

%% *****Physical parameters for the bottom*****
%% A two-layer model is implemented with a sediment fluid layer
%% over a solid half space
cp1=1700; ap1=0.5; rho1=1700;
p2=2500; ap2=0.5; rho2=2000;
cs2=0; as2=0;
lay_thick=10;
%% Specify the rms bottom or sea surface roughness ( in meters)
sigma_surface=0.0;
sigma_bottom=0.0;

%% *****Parameters for the ray tracing*****
%% Specifications of the angles for the initial ray tracing.
%% The initial launch angles at the source must be contained in
%% the vector start_theta (degrees);
%% Here is an example of 120 values from -32 to + 32 degree and
%% with a higher density of angles close to the horizontal direction,
%% which is often a good practice.
N_angle=32; theta_max=32; n=1:N_angle;
ang=theta_max.^(n/N_angle)-theta_max.^(1/N_angle) ;ang=ang(ang>0);
start_theta=sort([-ang ang]);
start_theta=start_theta(start_theta~=0);
%% Avoid starting a horizontal ray
%% Source array specification are introduced are 16 elements spaced
%% with 1 meter
Ne=16; delta_x=1;

%% Run this part if you want to add the previous stored
%% eigen angles in the start angles;
%% load eigen_angles;
%% eigen_angles=eigen_angles(eigen_angles~=0);
%% start_theta=[eigen_angles' start_theta];

%% The ray tracing will stop after "bottom_stop" bottom reflections
if %% not ==0 and after "surface_stop" surface reflections if
not ==0
bottom_stop=8; surface_stop=6
%% Stops after 8 bottom reflections or after 6 surface reflections

%% *****Accuracy and error control*****
%% The optional program findeigenray is controlled by
%% the parameters searcheigenray, N_iterations, eigprecision.
%% If para.searcheigenray==1 the search for eigenrays is iterative
%% stopping when the number of iterations reaches N_iterations or
%% the range error is less that eigprecision in meters
%% This routine may be quite time consuming to execute.
%% If the para.diagnostics==1 the program will at various stages
%% produces output which may be useful to locate errors
N_iterations=2; searcheigenray=1; searchrays=0; diagnostics=1;
eigprecision=3;
```

```
%%          DISPLAY and SIGNAL PROCESSING PARAMETERS*****

%% Sampling frequency fs for the calculation of the transfer function
and %%the time responses
%% Block length for the fourier transformr to time domain
%% Time window length is T_max=nfft/fs.
%% Watch out for aliasing errors in the time responses
fs =1024; nfft=1024;
%% gives 2 second of time signal;
%% The transmission loss as function of range is calculated for the
%% frequency specified in the vector
frequency=[ 100 200];
%% For high frequency applications you may specify the
carrier_frequency in Hz;
carrier_frequency=0;

%% There are two different range specifications; range_receiver and
%%range_phone.
%% range_receiver is the general specification used in the
%% calculations and should normally cover the whole range of the
scenario.
%% "range_phone "specifies the ranges for which the time responses
are
%% calculated and displayed and is normally a subset of
"range_receiver"
range_receiver =1:1:R_max; % Every 1 meter
range_phone=0:500:R_max; % Every 500 meter

%% Produces the contour plot of Figure 12% with transmission loss as
%% function of range and frequency
conplot=1;conplot=1;

%%*****end test case 0*****
%% case 123 %insert your new case here
%% The program package contains more cases

end % case selection

%% Keep rest of the file unchanged
rawinput.title_tekst=title_tekst;
rawinput.del_z = del_z;
rawinput.z_input= z_input;
rawinput.c_input = c_input;
rawinput.Rmax=R_max;
rawinput.N=N;
rawinput.z_source=z_source;
rawinput.z_receiver=z_receiver;
rawinput.delta_x=delta_x;
rawinput.Ne=Ne;
rawinput.z_max=z_max;
rawinput.range_source=range_source;
rawinput.rayopt=islinear;
rawinput.beamdisp = beamdisplacement;
rawinput.R_b=R_b;
rawinput.Z_b=Z_b;
rawinput.laythick=lay_thick;
rawinput.start_theta=start_theta;
rawinput.bottom_stop=bottom_stop;
rawinput.surface_stop=surface_stop;
```

```
rawinput.frequency=frequency;
rawinput.carrier_frequency=carrier_frequency;
rawinput.fs=fs;
rawinput.nfft=nfft;
rawinput.tlplot=tlplot;
rawinput.envplot=envplot;
rawinput.conplot=conplot;
rawinput.timeplot=timeplot;
rawinput.eigplot=eigplot;
rawinput.range_receiver=range_receiver;
rawinput.range_phone=range_phone;
rawinput.eigprecision=eigprecision;
rawinput.N_iterations=N_iterations;
rawinput.diagnostics=diagnostics;
rawinput.c_red=c_red;
rawinput.sigma_surface=sigma_surface;
rawinput.sigma_bottom=sigma_bottom;
rawinput.cp1=cp1;
rawinput.ap1=ap1;
rawinput.rho1=rho1;
rawinput.cp2=cp2;
rawinput.cs2=cs2;
rawinput.ap2=ap2;
rawinput.as2=as2;
rawinput.rho2=rho2;
rawinput.bothit=bothit;
rawinput.sspmethod=sspmethod;
rawinput.bathymethod=bathymethod;
rawinput.colbar=colbar;
rawinput.eigrange=eigrange;
rawinput.searcheigenray=searcheigenray;
rawinput.searchrays=searchrays;
rawinput.savememory=savememory;
rawinput.carrier_frequency=carrier_frequency;
%% end planerayinput
```



Technology for a better society